ADAPTIVE INVERSE MODELING OF A SHAPE MEMORY ALLOY

WIRE ACTUATOR AND TRACKING CONTROL WITH THE MODEL

A Thesis

by

BONG SU KOH

Submitted to the Office of Graduate Studies of
Texas A&M University
in partial fulfillment of the requirements for the degree of

MASTER OF SCIENCE

August 2006

Major Subject: Aerospace Engineering

ADAPTIVE INVERSE MODELING OF A SHAPE MEMORY ALLOY

WIRE ACTUATOR AND TRACKING CONTROL WITH THE MODEL

A Thesis

by

BONG SU KOH

Submitted to the Office of Graduate Studies of
Texas A&M University
in partial fulfillment of the requirements for the degree of

MASTER OF SCIENCE

Approved by:

Chair of Committee,	John L. Junkins
Committee Members,	Othon K. Rediniotis
	Darbha Swaroop
Head of Department,	Helen Reed

August 2006

Major Subject: Aerospace Engineering

ABSTRACT

Adaptive Inverse Modeling of a Shape Memory Alloy
Wire Actuator and Tracking Control with the Model. (August 2006)
Bong Su Koh, B.S., Korea Advanced Institute of Science and Technology
Chair of Advisory Committee: Dr. John L. Junkins

It is well known that the Preisach model is useful to approximate the effect of hysteresis behavior in smart materials, such as piezoactuators and Shape Memory Alloy(SMA) wire actuators. For tracking control, many researchers estimate a Preisach model and then compute its inverse model for hysteresis compensation. However, the inverse of its hysteresis behavior also shows hysteresis behavior. From this idea, the inverse model with Kransnoselskii-Pokrovskii(KP) model, a developed version of Preisach model, can be used directly for SMA position control and avoid the inverse operation. Also, we propose another method for the tracking control by approximating the inverse model using an orthogonal polynomial network. To estimate and update the weight parameters in both inverse models, a gradient-based learning algorithm is used. Finally, for the SMA position control, PID controller, adaptive controllers with KP model and adaptive nonlinear inverse model controller are compared experimentally.

TO MY FAMILY

ACKNOWLEDGMENTS

I am very thankful to my committee chair, Dr. John. L. Junkins, for the opportunity to work with him on this project and for his guidance. He showed me the way to go in my professional life because of his passion for knowledge and creativity. Similar gratitude is offered to the other members of my committee, Dr. Othon Rediniotis, who always showed the humor and intelligence and, Dr. Swaroop, who taught me about the world of nonlinear systems. I appreciate their guidance throughout the development of this thesis. Also, I thank my research team members, M. Majji and P. Singla, for helping me with pleasure. I would also like to thank my family for their support throughout my graduate studies. Finally, I would like to thank my wife for cheering me up to step forward.

TABLE OF CONTENTS

LIST OF FIGURES

Page

LIST OF TABLES

CHAPTER I

INTRODUCTION

Shape Memory Alloy(SMA) actuators have great advantages, namely large deformation, large pull force, and good recovery strain. With these benefits, a SMA actuator has been used for many diverse applications in robotics, medical instrumentation and the aerospace vehicle applications. For example, Hasimoto *et al.*[1] used SMA actuators for the biped walking robot. Ikuta[2] designed a micro/miniature SMA actuator for a gripper. J. Kudva[3] developed the SMA-actuated, hingeless, flexible leading and trailing edge control surface. F. K. Straub *et al.*[4] used two biaxial SMA tubes for in-flight blade tracking.

To model and control SMA actuators is not an easy problem because SMA actuators exhibit a thermomechanical behavior with large hysteresis due to temperature and applied force. To describe this nonlinear behavior, Ikuta *et al.*[5] proposed the variable sublayer model. Madrill and Wang[6] extended this model in order to explain the dynamic characteristics of SMA position control system. Brinson *et al.*[7] developed a different type of model based on the constitutive laws. This model can successfully describe the relationship among the stress, strain and temperature.

Another popular approach is the use of Preisach model. Many researchers have used this model to describe hysteretic phenomena of smart materials such as piezoelectrics and SMA actuators because a controller with hysteresis compensation can improve the performance of tracking control[8]. However, this model cannot express the drift due to cycling effect. Also, this model with identified parameters of weighting functions cannot predict the SMA deformation under the varying environments of the applied stress and ambient temperature. So, Webb *et al.*[9],[10] used the adaptive control method with the Krasnoselskii-Pokrovskii(KP) operator, a developed type of Preisach operator. This model can be updated continuously by using adaptive method so that it

_____

This thesis follows the style of *IEEE Transactions on Control System Technology*.

can describe the hysteresis behavior of an SMA wire actuator successfully under extended disturbances and various loading conditions. Moreover, by computing the inverse of it, the effect of the hysteresis in SMA actuator can be actively compensated.

This thesis uses a similar adaptive control technique with a KP hysteresis operator. However, in order to evade the computation of the inverse of the KP model, the inverse model with KP hysteresis operator can be directly used because the inverse of hysteresis behavior also has qualitatively the same characteristics of hysteresis. This property will be explained. These Preisach types of models require many computations and a lot of memory because of their model structure. These are a burden for the real time applications. So, we propose the nonlinear adaptive inverse model control by using an orthogonal function approximation to solve the SMA position control. This proves to be a more compact and computational attractive approach.

In this thesis, first, the characteristics of SMA wire actuator are studied. Second, the properties of Preisach types of hysteresis models and their operators are examined. Further, the adaptive control for the estimation of parameters in KP model will be validated. Finally, in experiments for the SMA position control, PID controller, adaptive controller with KP model, and adaptive nonlinear inverse model controller will be compared.

CHAPTER II

SHAPE MEMORY ALLOY(SMA)

This section introduces the material properties of shape memory alloy, thereby helping us to select the SMA wire actuators for appropriate applications.

A. *Characteristics of SMA*

The main property of SMA is the shape memory effect: If there is no applied force, the SMA is not deformed. However, this alloy is deformed easily at a low temperature by external forces. This deformed alloy can be restored to the original shape by the application of heat. These two different phases are called as Martensite and Austenite, respectively. From these observations, we can realize that the shape of SMA depends on the external stress and temperature. The effect of phase transformation on Ti-Ni is shown in Fig. 1[11].

This characteristic of SMA makes it a good candidate for use as a displacement actuator. Unfortunately, the relationship between temperature and strain exhibits a hysteretic phenomenon. This hysteresis prevents the use of SMA as a linear actuator.
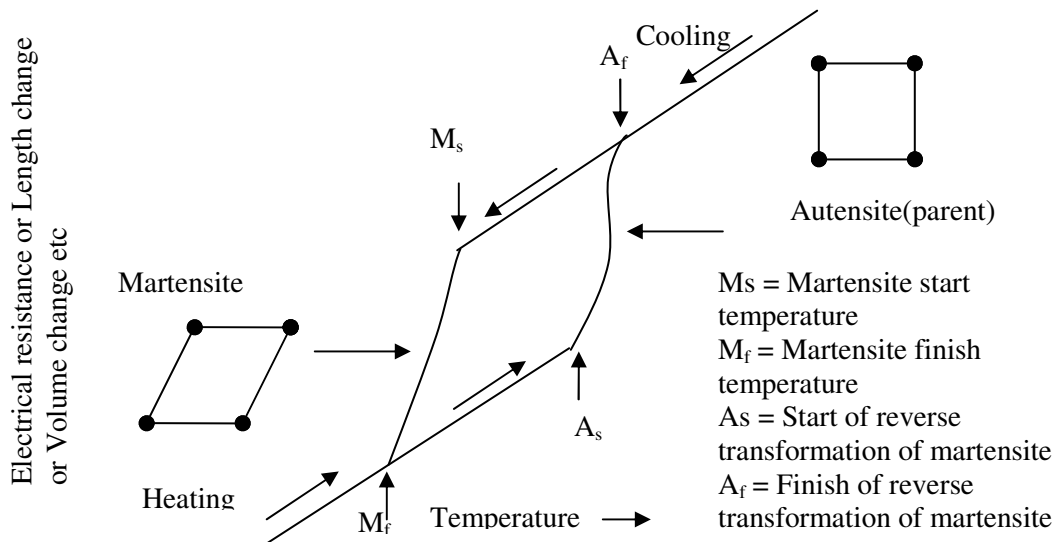
Fig. 1. Effect of phase transformation

B. *Cycling Effect*

The property of SMA by which its characteristics change due to repeated use is called the cycling effect. So, this effect should be considered for the design of signal inputs to the SMA for use as an actuator. The cycling effect results in the reduction of maximum available deformation and force. In case of Ti-Ni alloys, it is known that the available strain deformation changes from 7-8 % to 2-3% after 100,000 cycles.

C. *Properties of Ni-Ti Alloy Wire*

Table 1 shows the properties of Ni-Ti Alloy wire manufactured by DYNALLOY, Inc[12]. For the control application, these values should be carefully considered. If the diameter size is twice as large, then the maximum pull force increases about four times more. However, the cooling time(Off Time) and the current required for heating are also increasing. So, this table gives us guidance about SMA selection for control application.

Table 1

Properties of Ni-Ti Alloy

Diameter Size(Inches)	Resistance (Ohm/Inch)	Maximum Pull Force(gms)	Approximate current(mA)	Contraction time(Seconds)	Off Time 70ºC Wire(Seconds)
0.0010	45.10	7	20	1	0.10
0.0015	21.0	17	30	1	0.25
0.002	12.0	35	50	1	0.3
0.003	5.0	80	100	1	0.5
0.004	3.0	150	180	1	0.8
0.005	1.8	230	250	1	1.6
0.006	1.3	330	400	1	2.0
0.008	0.8	590	610	1	3.5
0.010	0.5	930	1000	1	5.5
0.012	0.33	1250	1750	1	8.0
0.015	0.2	2000	2750	1	13.0
0.020	0.16	3562	4000	1	17.0

D. *Heating and Cooling*

The passage of electric current causes the SMA material to heat. This has been used as an effective and popular method for temperature control. However, the resistance of an SMA wire is so small that large current is required for heating. From the table 1, Ni-Ti wire with 0.015'' diameter needs 2.75A approximately for heating at the room temperature. If the ambient temperature is low, the more current is required for heating. So, a large enough power supply should be selected for the control under the various environments. Also, the SMA wire must be electrically isolated from other surrounding objects as the current flowing directly through the SMA wire could cause a short circuit.

The cooling time determines the response time of the system. In order to increase the bandwidth of an SMA actuator, the effective cooling method should be employed. The following methods have been examined: forced convection cooling(with fan), cooling with running water, ice cooling, and cooling with a Peltier element or heat sink. Each method has advantages and disadvantages. M. Hashimoto *et al.*[13] show the cooling curves for various cooling methods with 0.8 Ti-Ni wires. This graph explains that the heat sink and water cooling method can have a faster response than air-cooling and ventilation with 1.0 m/s. However, the heat sink and water cooling method need other complex hardware for installation.

In our application, an SMA wire actuator with 0.012'' diameter has been used.

CHAPTER III

CLASSICAL HYSTERESIS MODEL

In this section, the relationship between hysteresis and its inverse will be examined. Also, the concept and features of the classical Preisach model and modified Preisach model will be presented. A detailed coverage of the material in this section may be found in the reviews[14],[15].

A. *Relationship between Hysteresis and Its Inverse*

(a)   (b)
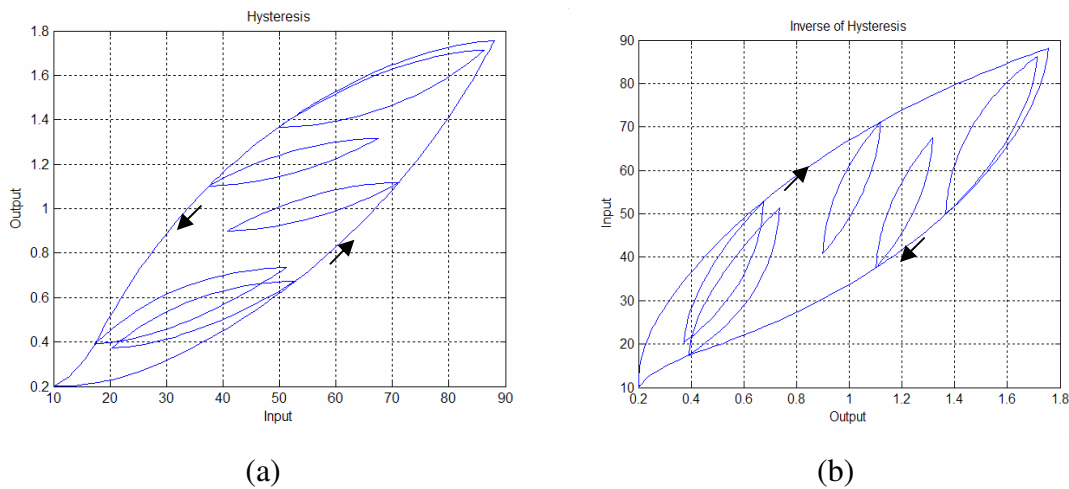
Fig. 2. Hysteresis and its inverse

The figures represent a one to one mapping between the input and output of a hysteretic system. In the SMA wire, the relationship between the temperature and the displacement yields such a hysteresis behavior. In SMA control application, many researchers used Preisach models to describe the hysteresis behavior of SMA actuators and compensate for it by computing the inverse model as depicted above. However, if we want only tracking control of SMA wire, it is possible to obtain the direct inverse model with Preisach model to avoid the inverse operation. M.M. Khan *et al.*[16] show that the relationship between strain and stress has a type of hysteresis represented in Fig.

2 (b), and they use the Preisach model for describing this relationship[16]. From this observation, we can conclude that the Preisach model can describe several types of hysteresis in Fig. 2. Such a classical Preisach model is introduced below.

B. *Classical Preisach Model*

The classical Preisach model can be written as follows

$$f(t) = \iint_{\alpha \geq \beta} \mu(\alpha, \beta)\hat{\gamma}_{\alpha\beta}u(t)d\alpha d\beta \tag{1}$$

where $u(t)$ is the input and $f(t)$ is the output, and $\hat{\gamma}_{\alpha\beta}$ is the elementary hysteresis operator which represents the hysteresis nonlinearities with local memories[14]. In our case, the input is the temperature of the SMA wire and the output is the displacement of the SMA wire. The function $\mu(\alpha, \beta)$, called Preisach function, is an arbitrary weight function over the Preisach Plane described as $P = \{(\alpha, \beta)|\alpha \geq \beta\}$. If this Preisach function is known from the experiment, the above equation can model the hysteresis. Therefore, to construct the Preisach function from the experimental data, we use an identification process.

From Eq. (1), this model can be considered as a system with parallel connected relays. This interpretation is explained in Fig. 3. From this figure, the input $u(t)$ is applied to each relay which has its own switching pair values (α_i, β_i) over the Preisach plane and then multiplied by the weight function. After these multiplications, those outputs are integrated. This is the output of the Preisach model.
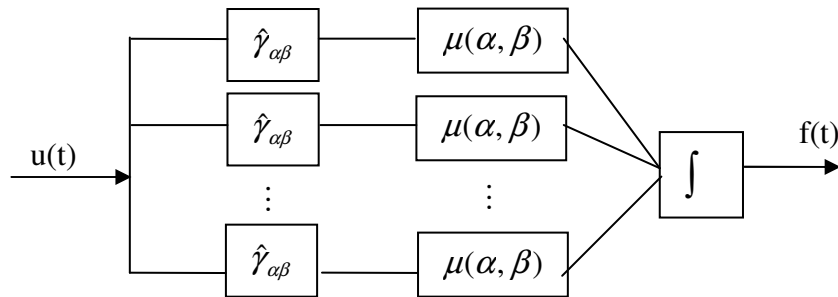

Fig. 3. Classical Preisach model

The function of each relay operator is explained as shown in Fig. 4. The values of α and β represent the switching values, "up" and "down", respectively. When the input $u(t)$ increases monotonically above the value of α, $\hat{\gamma}_{\alpha\beta}u(t)$ has the "+1". And, when the input $u(t)$ decreases monotonically below the value of β, $\hat{\gamma}_{\alpha\beta}u(t)$ has the "-1". This means that each relay operator has only "+1" or "-1".

M. M. Khan *et al.*[16] suggest the modified relay operator to describe the SMA tube undergoing tension or compression. This modified relay operator has "+1" or "0" instead of "+1" and "-1". It can apply to our application with SMA wire because the displacement has the only positive value.

(a) Classical Preisach operator   (b) Modified relay operator
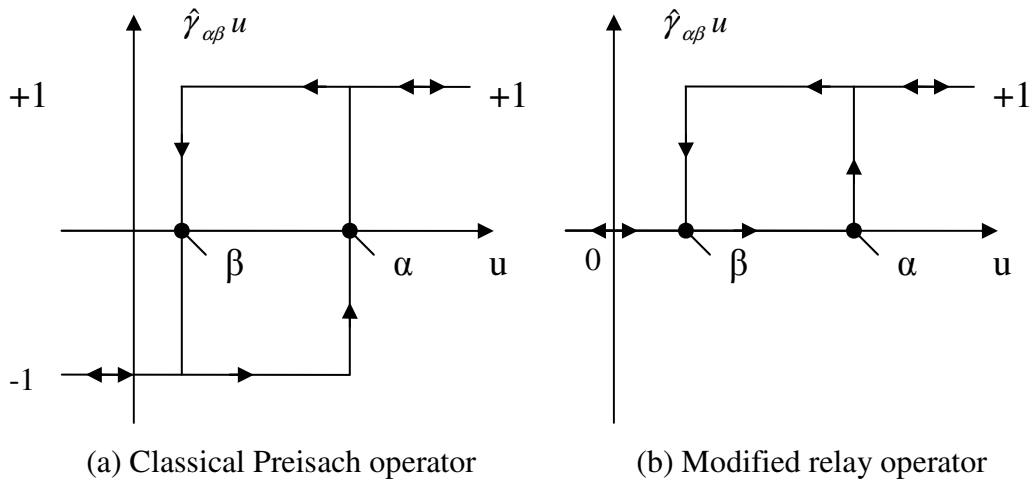
Fig. 4. Relay operator

C. *Geometric Interpretation of the Classical Preisach Model*

Fig. 5 shows the Preisach plane. The weight function $\mu(\alpha, \beta)$ has "0" in the outside of right triangular T in Fig. 5. Each point (α_i, β_i) in the Preisach plane has its only one particular relay operator $\hat{\gamma}_{\alpha\beta_i}$. This means that the relationship between point (α_i, β_i) and hysteresis operator is a one-to-one correspondence. Therefore, if we define the Preisach plane and find the weight function from experiments, our Preisach model is complete.
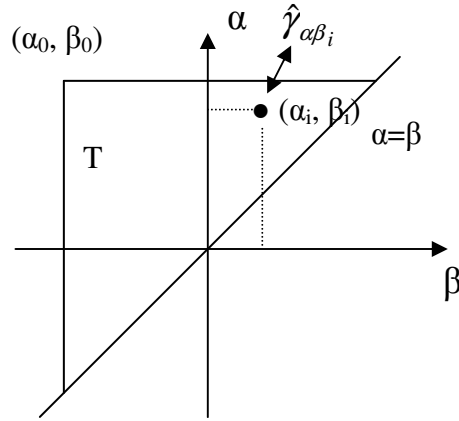
Fig. 5. Preisach plane

Let us explain how this Preisach model can work by using Preisach plane in Fig. 6. First, assume that the input $u(t)$ has the value below the value of β_0. In this case, all Preisach operators $\hat{\gamma}_{\alpha\beta}$ values in the right triangular T have the "-1". When the input $u(t)$ increases monotonically to some maximum value u_1 as in Fig. 6(a), $\hat{\gamma}_{\alpha\beta}$ operators in the S^+ turn into "+1". At this time, the other area in the T is denoted by the S^-, and $\hat{\gamma}_{\alpha\beta}$ operators in this area still have "-1". When the input $u(t)$ decreases monotonically to some minimum value u_2, the S^- area increases. Whereas the S^+ area decreases as shown in Fig. 6(b). If we have the input history described in Fig. 6(d), the S^+ area and the S^- area in the Preisach Plane can be divided as shown in the Fig. 6(c). And, relay operators in the S^+ have "+1" and $\hat{\gamma}_{\alpha\beta}$ operators in the S^- have "-1".

Thus, Preisach Plane has two types of area with $S^+(t)$ and $S^-(t)$ at any instant of time in the T. Each of them has the points (α, β) which have the corresponding relay operators with "+1" and "-1", respectively. From this interpretation, Eq. (1) can be subdivided into two integrals.
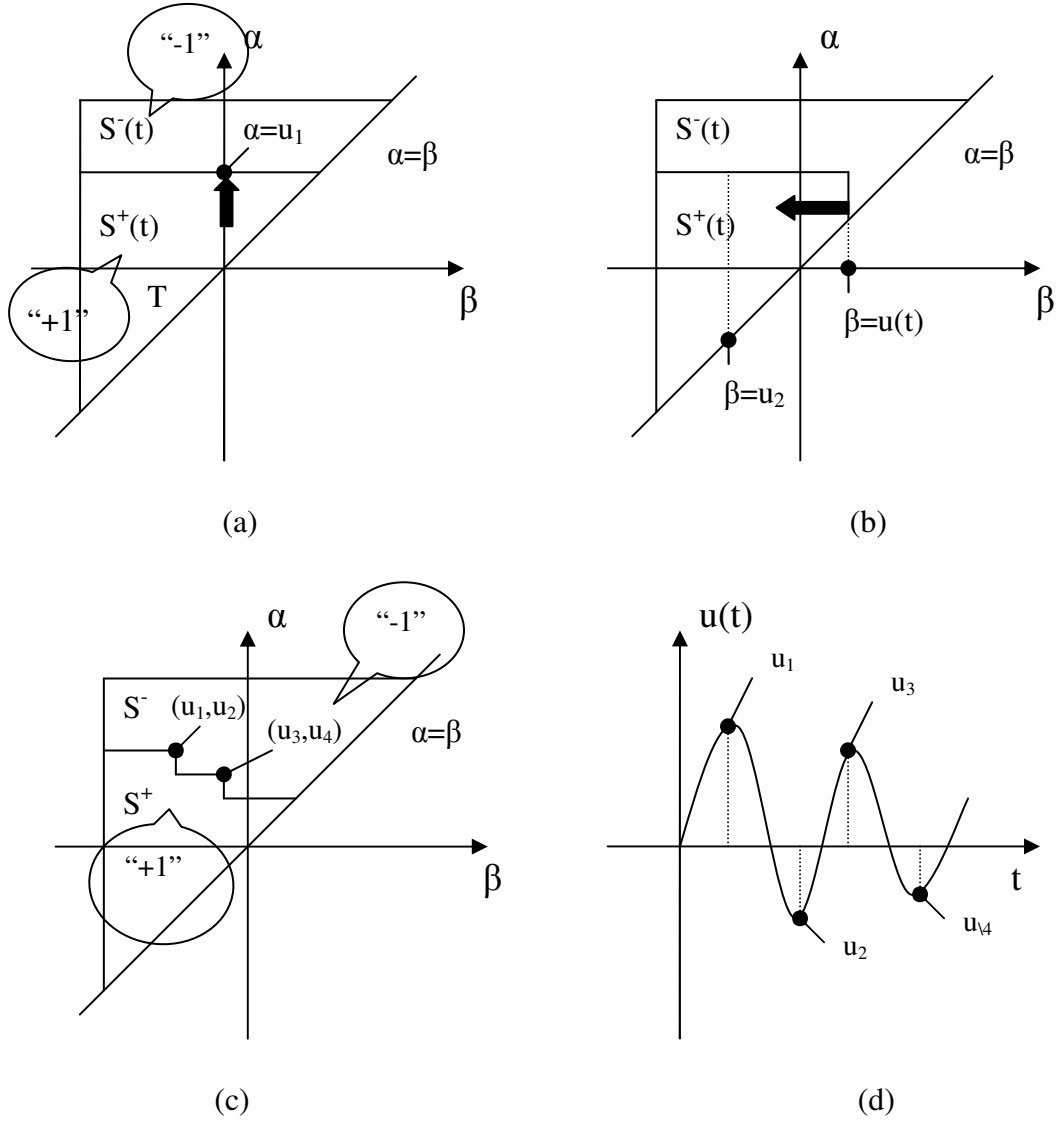
Fig. 6. Preisach plane and input history

$$f(t) = \iint_{S^+(t)} \mu(\alpha, \beta)\hat{\gamma}_{\alpha\beta}u(t)d\alpha d\beta - \iint_{S^-(t)} \mu(\alpha, \beta)\hat{\gamma}_{\alpha\beta}u(t)d\alpha d\beta \qquad (2)$$

Because the $\hat{\gamma}_{\alpha\beta}u(t)$ is "+1" with points (α, β) in the $S^+(t)$ and $\hat{\gamma}_{\alpha\beta}u(t)$ is "-1" with points (α, β) in the $S^-(t)$, the Eq. (2) can be written by

$$f(t) = \iint_{S^+(t)} \mu(\alpha, \beta)d\alpha d\beta - \iint_{S^-(t)} \mu(\alpha, \beta)d\alpha d\beta \qquad (3)$$

For the modified hysteresis relay operator, $\hat{\gamma}_{\alpha\beta}u(t)$ is "0" in the $S^-(t)$. So, Eq. (2) and Eq. (3) can be written as

$$f(t) = \iint_{S^+(t)} \mu(\alpha,\beta)\hat{\gamma}_{\alpha\beta}u(t)d\alpha d\beta \tag{4}$$

$$f(t) = \iint_{S^+(t)} \mu(\alpha,\beta)d\alpha d\beta \tag{5}$$

This classical Preisach model has the following two important properties. First is the *wiping-out property*[14]. This property represents that Preisach model only stores the alternating dominant input extrema. Second is the *congruency property*[14]. This property tells that if the input is continuously changing between two consecutive extremum values, the corresponding outputs are congruent. These properties can be the important criteria for the possibility when we apply the smart material to the Preisach model. For SMA, D. Hughes and J. Wen[17] verify these properties experimentally.

D. *Properties of Preisach Model for Inverse of Hysteresis*

If the each weight fuction has a positive value over the Preisach plane, the input-output graph has the property described in Fig. 2(a). However, to get the characteristic of hysteresis like Fig. 2 (b), some analysis about the weight function of Preisach model is required.
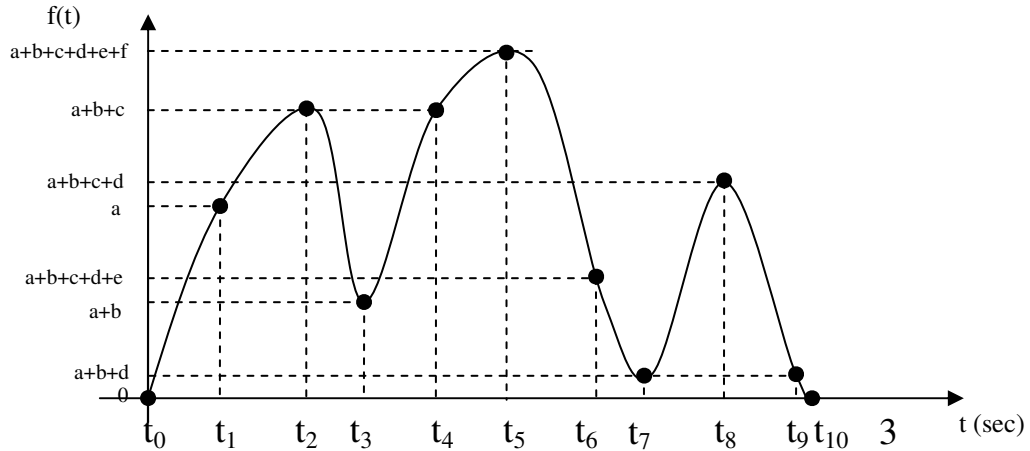

Fig. 7 Output history of hysteresis

Fig. 7 represents the output history of hysteresis like Fig 2(b). The corresponding Preisach plane and input-output graph are shown in Fig. 8.
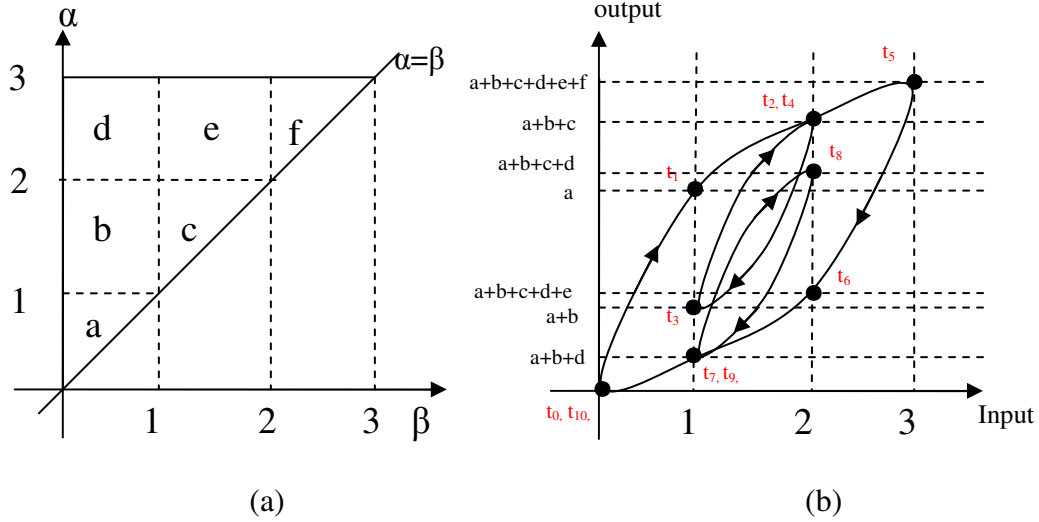

(a)   (b)

Fig. 8. Preisach plane and its input-output graph

From Fig. 8(a) and Eq. (1), the output of hysteresis at t_3 is following as

$$f(t) = \iint\limits_{\alpha \geq \beta} \mu(\alpha, \beta)\hat{\gamma}_{\alpha\beta}u(t)d\alpha d\beta$$

$$= \int_0^1\int_\beta^1 \mu(\alpha, \beta)\hat{\gamma}_{\alpha\beta}u(t)d\alpha d\beta + \int_0^1\int_1^2 \mu(\alpha, \beta)\hat{\gamma}_{\alpha\beta}u(t)d\alpha d\beta + \int_1^2\int_\beta^2 \mu(\alpha, \beta)\hat{\gamma}_{\alpha\beta}u(t)d\alpha d\beta +$$

$$\int_0^1\int_2^3 \mu(\alpha, \beta)\hat{\gamma}_{\alpha\beta}u(t)d\alpha d\beta + \int_1^2\int_2^3 \mu(\alpha, \beta)\hat{\gamma}_{\alpha\beta}u(t)d\alpha d\beta + \int_2^3\int_\beta^3 \mu(\alpha, \beta)\hat{\gamma}_{\alpha\beta}u(t)d\alpha d\beta$$

$$= a + b + c + d + e + f$$

(6)

At each time t_k, $\{k \in 1,2,3,4,5,6,7,8,9,10\}$, we can express the output value with a, b, c, d, e and f in Fig. 8(a). The relationship between these outputs is shown in Fig. 8(b). As a result, we can introduce the relative value and sign of the weight function $\mu(\alpha, \beta)$ from Fig. 8(b). These relationships are expressed as

$$a + b + c + d + e + f > a + b + c > a > 0$$

$$\therefore d + e + f > 0, b + c > 0, a > 0, b + c + d + e + f > 0$$

(7)

$$a + b + c + d + e + f > a + b + c + d + e > a + b + d > 0$$

$$\therefore f > 0, c + e > 0, c + e + f > 0, a + b + d > 0 \tag{8}$$

$$a > a + b > a + b + d > 0 \therefore 0 > b, 0 > d, -b > d, a + b + d > 0 \tag{9}$$

$$a + b + c > a + b + c + d > a + b + c + d + e > 0$$

$$\therefore 0 > d, 0 > e, (d + e) > -(a + b + c) \tag{10}$$

From Eq. (7) – (10), we can verify the important properties. These properties give us intuition about the weight function of the hysteresis like Fig. 2(b). So, these properties can help in guessing the initial values of weight function for adaptive identification. This will be discussed later.

As a result, we can express both types of hysteresis described in Fig 2 by using the Preisach model.

CHAPTER IV

KRASNOSELSKII-POKROVSKII(KP) INTEGRAL HYSTERESIS MODEL

The KP integral hysteresis model has better properties for real time control application. The KP operator is developed from the classical Preisach operator[18]. The value of each elementary hysteresis operators is obtained from the integration over a class of kernels. Also, the gradient algorithm about the on-line identification for the KP model is examined. We demonstrate this with a simulation. Finally, gradient method can find the KP model or the direct inverse model with the KP model in the well-defined problem. The KP model is discussed in further detail in [15],[19],[20].

A. *Modified Preisach Operator*

Fig. 4(b) shows the modified Preisach operator. The classical Preisach operator is explained in [15]. In our case, some modifications will be presented to describe the modified Preisach model. The following is the mathematical representation of the modified Preisach model.

The kernel of the modified Preisach operator is represented by

$$[\hat{\kappa}(u,\xi)](t) = \begin{cases} [\hat{\kappa}(u,\xi)](0) & if & T_c(t) = \phi \\ 0 & if \ T_c(t) \neq \phi & and & u(\max(T_c(t))) = \beta \\ 1 & if \ T_c(t) \neq \phi & and & u(\max(T_c(t))) = \alpha \end{cases} \quad (11)$$

where u(t) is the input, $\xi \in \{0,1\}$ is the initial state of the operator. Also, $S = \{s \in R^2 : s = (\beta,\alpha), \alpha > \beta\}$ is the set of pairs of switching values and the crossing time is defined as $T_c(t) = \{\eta \in (0,t] : u(\eta) = \beta \ or \ u(\eta) = \alpha\}$ [15]. This means that T_c has the time values whenever the input is crossing the switching values. The initial state of the delayed relay operator is given by

$$[\hat{\kappa}(u,\xi)](0) = \begin{cases} 0 & if \ u(0) \leq \beta \\ \xi & if \ \beta < u(0) < \alpha \\ 1 & if \ u(0) \geq \alpha \end{cases} \quad (12)$$

B. *KP Operator*

For any monotone function, the output operator is defined by

$$\kappa(u,\xi) = \begin{cases} \max(\xi, r(u-\alpha)) & \dot{u} > 0 \\ \min(\xi, r(u-\beta)) & \dot{u} < 0 \\ \kappa\big|_{previous} & \dot{u} = 0 \end{cases} \tag{13}$$

where u(t) is the input and $\xi \in \{0,1\}$ is the initial state of the operator[15]. Also, $r(x)$ is locally a Lipschitz continuous ridge function, as shown in Fig. 9. In our case, this function is defined mathematically by

$$r(x) = \begin{cases} 0 & x < 0 \\ \dfrac{x}{a} & 0 \le x \le a \\ 1 & x > a \end{cases} \tag{14}$$
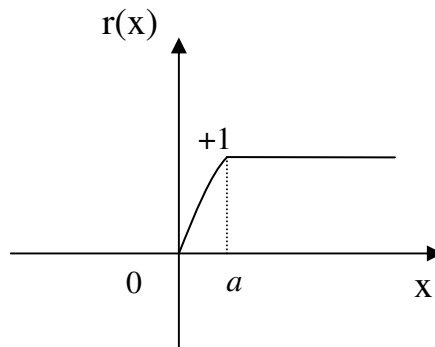
Fig. 9. Ridge function

For all functions with $u \in C[0,T]$, the KP kernels can be extended. This work is discussed in literature[15]. The kernel of the Preisach operator is only piecewise continuous in time, whereas the KP operator is continuous in time and parameter space[19]. As a result, the KP operator is useful in deriving a convergent approximation for the identification problem of a hysteretic behavior. The proof about this continuous mapping is shown in reference[15].

C. *Parameterized KP Model*

The KP integral model is the continuous form, but, for practical application, it needs a lot of computation time. So, the discretized KP model for the SMA actuator was developed by G. Webb[15]. The following explanation is the summary of KP model developed.

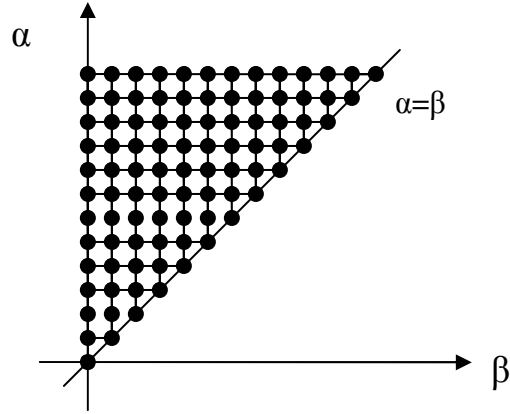Fig. 10. Preisach plane in parameterized KP model

First, the Preisach plane $P = \{(\alpha,\beta)|\alpha \geq \beta\}$ is discretized into a mesh grid as shown in Fig. 10. Each grid point in the Preisach plane is denoted by $s_i = (s_1, s_2)_i$, and the corresponding kernel function $\kappa_{s_{ij}}(u, \xi_{ij})$ should be discretized. Thus, the output of the discretized KP integral model is written by

$$y(u) = \sum_{i=1}^{K}\sum_{j=i}^{K}[\kappa_{s_{ij}}(u, \xi_{ij})](t) \cdot \theta_{ij} \tag{15}$$

where K is parameterization number which decides the number of grids in the vertical or horizontal line over the Preisach plane, $s_{ij} = (s_{1i}, s_{2j})$, ξ_{ij} is the inner loop memory for s_{ij}, θ_{ij} is the weighting value of the discretized form of the weight function $\mu(\alpha, \beta)$ and $\kappa_{s_{ij}}(u, \xi_{ij})$ is the kernel function represented by

$$\kappa_{s_{ij}}(u, \xi_{ij}) = \begin{cases} \max(\xi_{ij}, r(u - sj)) & \dot{u} > 0 \\ \min(\xi_{ij}, r(u - si)) & \dot{u} < 0 \\ \kappa_{s_{ij}}\big|_{previous} & \dot{u} = 0 \end{cases} \tag{16}$$

This kernel operator was explained in the previous chapter. The output of this KP model will be denoted as $Y_{KP}(u)$.

$$Y_{KP}(u) = \sum_{i=1}^{K}\sum_{j=i}^{K}[\kappa_{s_{ij}}(u, \xi_{ij})](t) \cdot \theta_{ij} \tag{17}$$

The above equation can be written as the vector form for more convenience in adaptive identification.

$$Y_{KP}(u) = \Theta^T K_{KP}(u) \tag{18}$$

where Θ is the parameter vector and is defined as

$$\Theta = [\theta_{11}, \theta_{12}, \theta_{22}, \cdots, \theta_{KK}]^T \in \mathfrak{R}^N \tag{19}$$

And, $K_{KP}(u)$ is the vector function and is defined as

$$K_{KP}(u) = [\kappa_{s_{11}}(u, \xi_{11}), \kappa_{s_{12}}(u, \xi_{12}), \kappa_{s_{22}}(u, \xi_{22}), \cdots, \kappa_{s_{KK}}(u, \xi_{KK})]^T \in \mathfrak{R}^N \tag{20}$$

where N is not only the dimension of Θ and $K_{KP}(u)$ but also the number of grid points, s_{ij}, which is obtained from the relationship by

$$N = \frac{K(K+1)}{2} \tag{21}$$

D. *Gradient Algorithm for the Recursive Identification of Hysteresis*

As mentioned before, the parameterized KP hysteresis model is represented by

$$y = Y_{KP}(u) = \theta^T K_{KP}(u) \tag{22}$$

For the estimation of parameter θ, our estimator is generated as

$$\hat{y} = \hat{Y}_{KP}(u) = \hat{\theta}^T K_{KP}(u) \tag{23}$$

where $\hat{\theta}$ is the estimate of θ at each time t. The estimation error e_1 is created as

$$e_1 = y - \hat{y} \tag{24}$$

To minimize it with respect to θ, we use the update law of normalized gradient algorithm[21].

$$\dot{\hat{\theta}} = \frac{\gamma e_1 K_{KP}(u)}{m^2} \tag{25}$$

where $m^2 = 1 + K_{KP}(u)^T K_{KP}(u)$.

When we know *a priori* about bound on parameter θ, the update law can use this information. The normalized gradient algorithm with projection[21] is expressed by

$$\dot{\hat{\theta}}_j = \begin{cases} f_j & if \ \theta_j \in [\Theta_j^a, \Theta_j^b] \quad or \quad \theta_j = \Theta_j^a, f_j \geq 0 \quad or \quad \theta_j = \Theta_j^b, f_j \leq 0 \\ 0 & otherwise \end{cases} \tag{26}$$

where $f_j = \frac{\gamma e_1 K_{KP}(u)_j}{m^2}$, $\theta \in \mathfrak{R}^n$ and $j = 1,...,n$.

E. *Simulation Study*

From the following example, we can guarantee that any type of hysteresis shown in Fig 2. can be described with the direct inverse model of hysteresis with the KP model. First, input and output data from the KP hysteresis model like Fig. 2(a) are generated. Then, input and output data exchange for getting the direct inverse model with a KP hysteresis model.

The specifications of the KP hysteresis model are the following. The model has N=210 KP operators and the parameter a of the ridge function in KP kernel is 5. The input is given as

$$u(t) = 45 + 25\sin(0.5\pi t)\cos(0.8\pi t) \tag{27}$$

The input should be *persistent excitation*(PE) for parameter convergence of the adaptive control. Fig. 11 represents the input and output from the KP model.
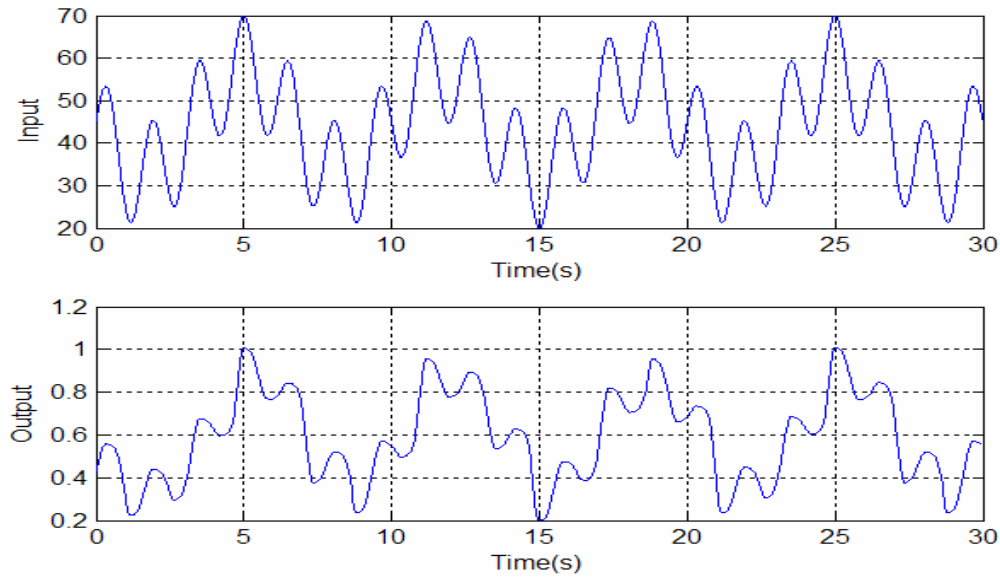
Fig. 11. Input and output signal from KP model

The inverse model with a KP hysteresis model has N=136 operators and parameter a of the ridge function in KP kernel is 0.066. The input range is from 0.1 to 1.09. In Fig. 11, the input and output are exchanging for this model. The initial values of weight function are given by the following equations.

$$\theta_{ij} = \begin{cases} -0.8 + i \times 0.01 & if \quad i > j \\ 12 - i \times 0.3 & if \quad i = j \end{cases} \tag{28}$$

where i and j are the index of switching values, α and β, in the parameterized KP Plane, respectively. Fig. 12 shows these values roughly. Because of $\alpha \geq \beta$ in Fig. 12, $i \geq j$ in $i \in \{1,..., K\}$, $j \in \{1,..., K\}$. And K is chosen as16. This guess may be obtained from the information about the relationships between values of weighting function in the chapter III.
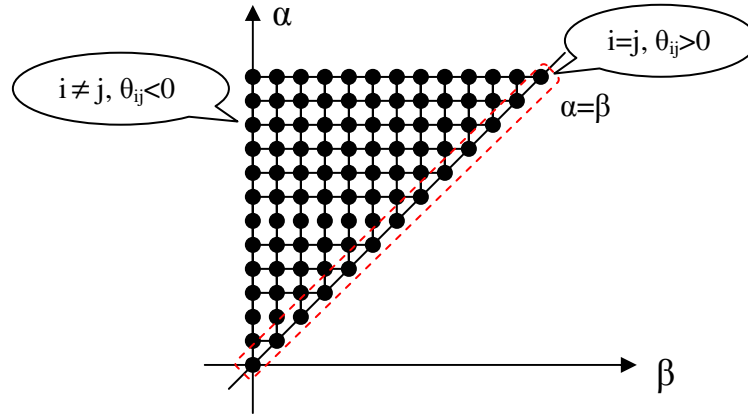
Fig. 12. Initial values in KP plane

The update law of normalized gradient algorithm with projection is used for the adaptation of the θ_{ij} weight function. The adaptation gain γ is selected as 20.

$$\dot{\hat{\theta}}_{ij} = \begin{cases} f_{ij} & if & i = j \quad and \quad \{\theta_{ij} > 0 \quad or \quad \theta_{ij} = 0, f_{ij} \geq 0\} \\ f_{ij} & if & i \neq j \quad and \quad \{\theta_{ij} < -0.01 \quad or \quad \theta_{ij} = -0.01, f_{ij} \leq 0\} \\ 0 & otherwise \end{cases} \quad (29)$$

where $f_{ij} = \dfrac{\gamma e_1 K_{KP}(u)_{ij}}{m^2}$ and $m^2 = 1 + K_{KP}(u)^T K_{KP}(u)$.

Fig. 13 shows that the hysteresis response with adaptive update. The adaptive KP model can follow the hysteresis plant well. If the adaptation gain γ is large, the adaptation is faster[22]. Fig. 14 represents the output prediction of the KP model with the updated parameters shown in Fig. 15. This fixed model can also predict the hysteresis output with reasonable error. These relationships between the input and output in both cases are shown in Fig. 16.
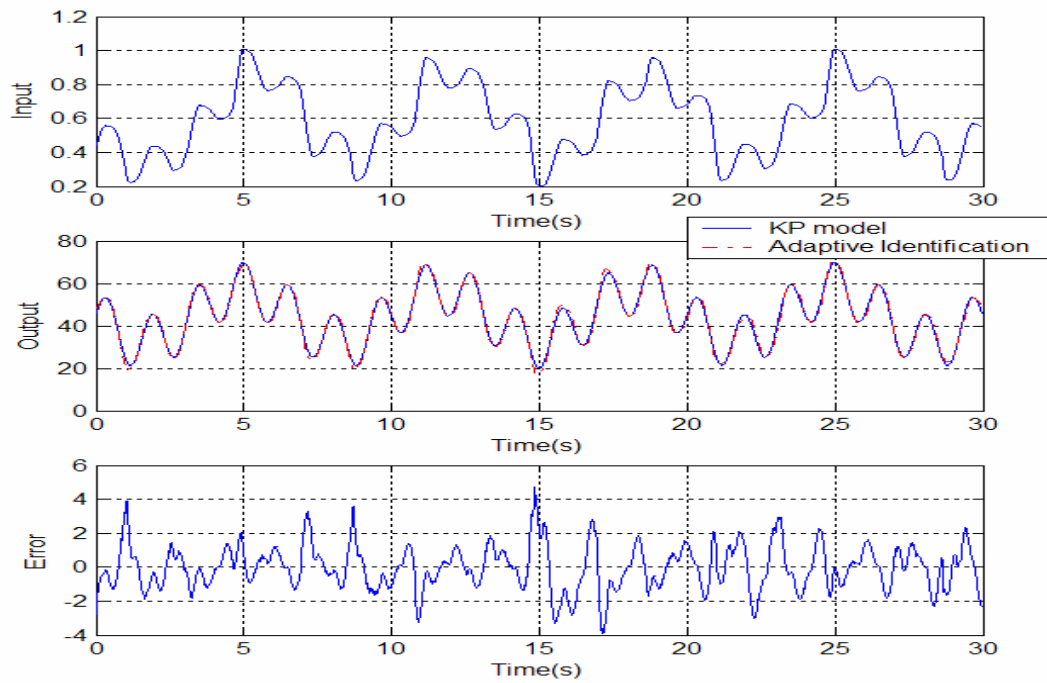
Fig. 13. Adaptive identification of KP model
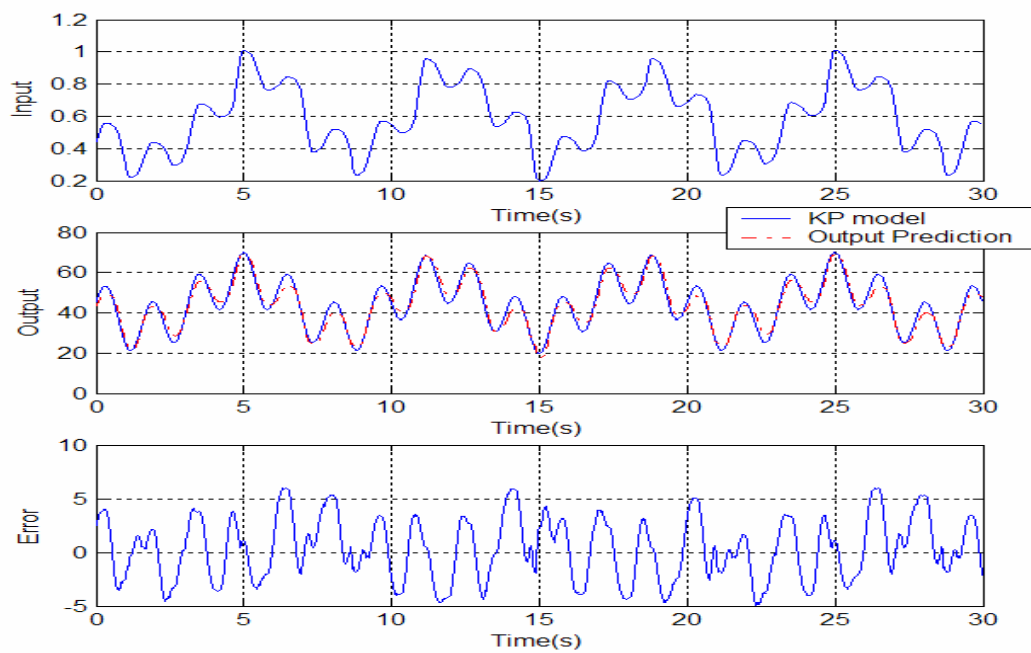

Fig. 14. Output prediction with a fixed KP model
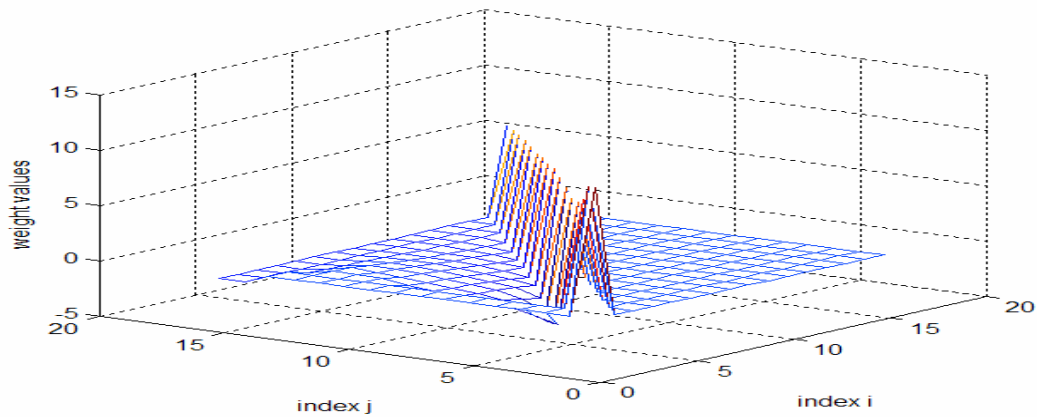
Fig. 15. Weight values of KP model after adaptation of 30 seconds
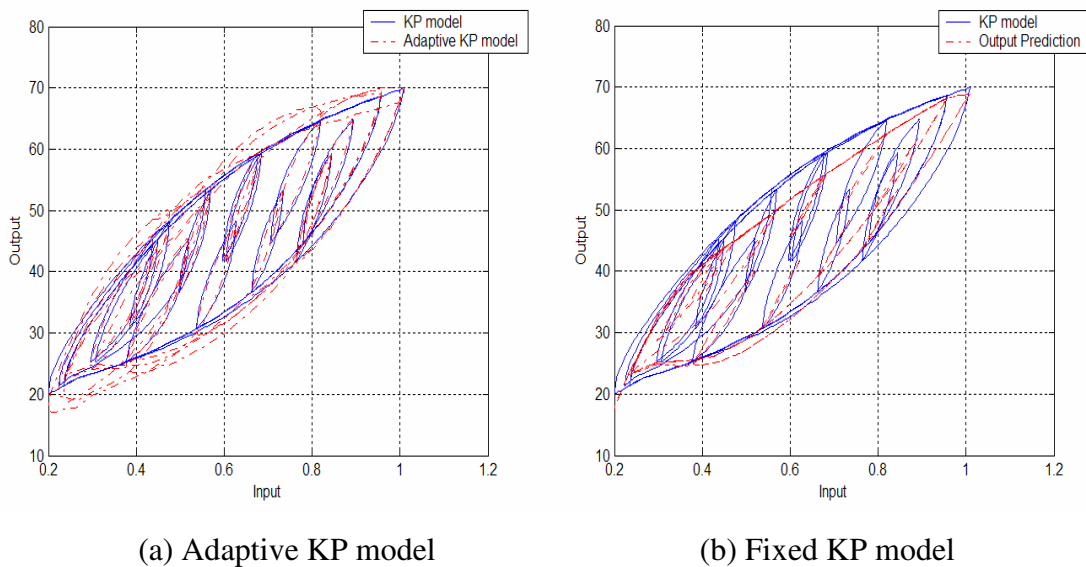
(a) Adaptive KP model   (b) Fixed KP model

Fig. 16. Hysteresis response

Generally, the hysteresis model has the shape and the movement direction of Fig. 2(a). For the tracking problem, many researchers found the hysteresis model and its inverse model. From the above results of simulation, any types of hysteresis shown in Fig. 2 can be helpfully described with the direct inverse model of hysteresis with the KP model and utilize it for the tracking control without the process of obtaining its inverse model.

CHAPTER V

CONTROL OF SMA WIRE ACTUATOR

A. Experimental Setup

Fig. 17. Schematic of SMA wire actuator

Fig. 17 represents the schematic and data flow for the control of an SMA wire actuator. SMA wire is fixed to the top of the te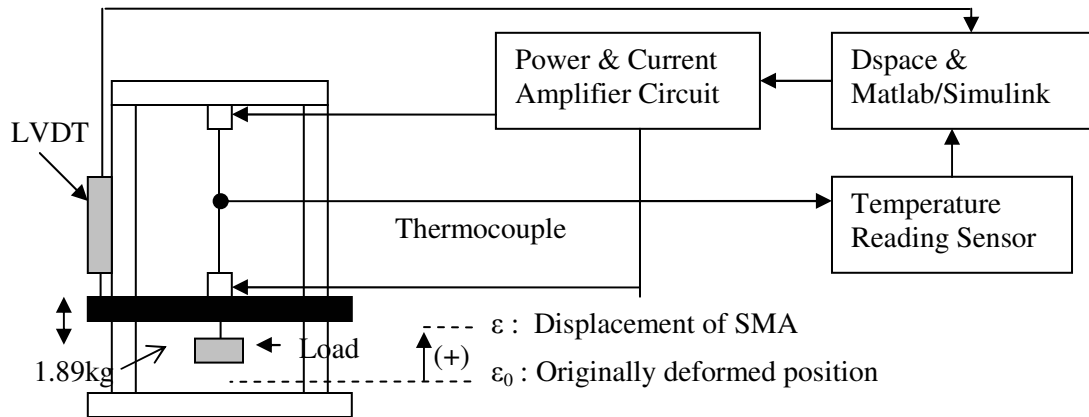st frame and the other end is connected to the load which is free to move vertically. Linear Variable Displacement Transducer(LVDT) can measure the absolute displacement ε of an SMA wire. The sign of the displacement is assigned positive when the load is moving upward, and the K-type thermocouple sensors the temperature of the SMA wire through the temperature reading circuit designed by using AD595AC. To amplify the current, the power amp transistor, MJE3055T, is used. More detail circuit diagram is shown in the appendix A.

To implement the real time control, dSPACE Data acquisition and Matab/Simulink are used. dSPACE Data Acquisition provides the input control signal with low current. This input signal with low current is amplified through the current amplifier circuit, and then supplied to the SMA wire actuator. The SMA wire used in our experiment is Nickel-Titanium SMA wire with 1 foot in length and 0.012'' in diameter.

The weight of the load applied acts as the restoring force on the SMA wire back to its original position.

B. Heat Transfer and Temperature Control

In our KP model, the input is temperature, and the output is SMA displacement. However, when we want to heat the SMA wire, we cannot increase the temperature directly. So, a heat source is required. This means that even if we can get the right input prediction, we cannot give it to the plant directly. In our experiment, by controlling a voltage from the power supply into the SMA wire, a desired temperature is attained.

To know the heat transfer equation of the SMA wire, we assume that only natural convection occurs. From many researches, it is well known that a heat equation of SMA wire as follows.

$$\dot{T} = -\frac{h}{\rho c}(T - T_\infty) + \frac{1}{\rho c}Q_{gain} \tag{30}$$

where h is the convection heat transfer coefficient, ρ is the mass density of the SMA wire, c is the specific heat of the SMA wire, and T_∞ is the ambient temperature[15].

Our electrical energy Q_{gain} from our experimental setup can be expressed as a function of both value of resistor and an applied voltage or current.

$$Q_{gain} = Ri^2 = \frac{V^2}{R} \tag{31}$$

The temperature of the SMA wire is governed by the following heat transfer equation.

$$\dot{T} = -\frac{h}{\rho c}(T - T_\infty) + \frac{1}{\rho c}\frac{V^2}{R} \tag{32}$$

The above equation can be given by

$$\frac{d\bar{T}}{dt} = -a\bar{T}(t) + bu(t) \tag{33}$$

where $a = \dfrac{h}{\rho c}$, $b = \dfrac{1}{\rho cR}$, $\bar{T} = T - T_\infty$ and $u = V^2$.

Generally, many researchers assume that h and c are constant. However, it is known that h and c are temperature dependent for an SMA wire[23],[24]. Also, parameter R changes during the transformation of the SMA between martensite and austenite phases. So, in the above equation, a and b are temperature dependent. Therefore, it is complex to determine the parameters exactly. However, without any complex experiments, we can get a good tracking result of temperature by using Proportional Integral and Derivative(PID) controller. This temperature tracking problem is also solved by using an adaptive Model Reference Control(MRC)[15].

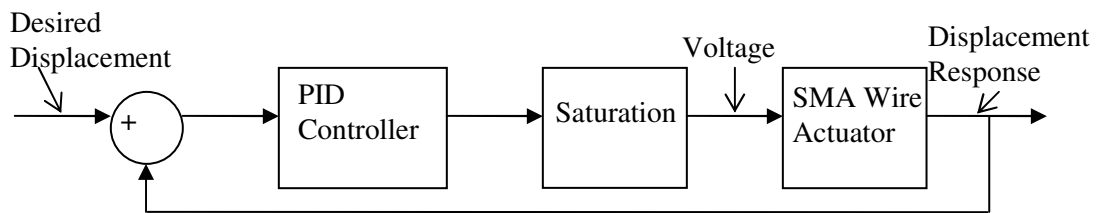*C. PID Feedback Controller for Temperature and Displacement Tracking Control*

Fig. 18. Schematic of PID closed loop controller

A PID controller is easy to implement. Traditionally, PID controllers are known for their robustness properties. In our experiment, we have the two kinds of PID controllers. One is used for displacement tracking control when we use the PID controller as a SMA position controller in Fig. 18. Another one is used for temperature control. PID controller used for tracking control does not require temperature control, whereas adaptive controllers with inverse models need the temperature control because their models have the relationship between temperature and displacement. For these two objectives, a PID feedback controller is used.

PID controller in the Laplace domain can be described as

$$Y(s) = K_P + \frac{K_I}{s} + sK_D \tag{34}$$

where K_P is the proportional gain, K_I is the integral gain and K_D is the derivative gain.

After some repeated experiments, we can adjust these three gains for good results.
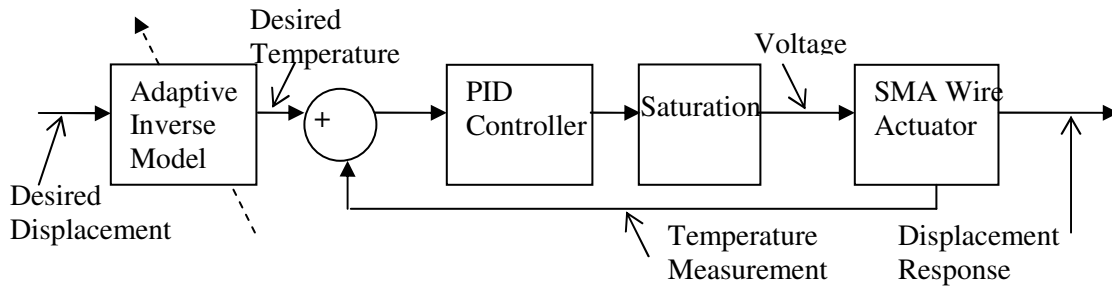
D. *Control Methodology for Adaptive Controller*

Fig. 19. Schematic of adaptive controller

With the adaptive algorithm studied from the previous chapter, the KP model can be used as a tracking controller for prediction of input. Also, the adaptive inverse model with an orthogonal polynomial network will be used. This will be explained in the next section. Both adaptive controllers have the schematic in Fig. 19.

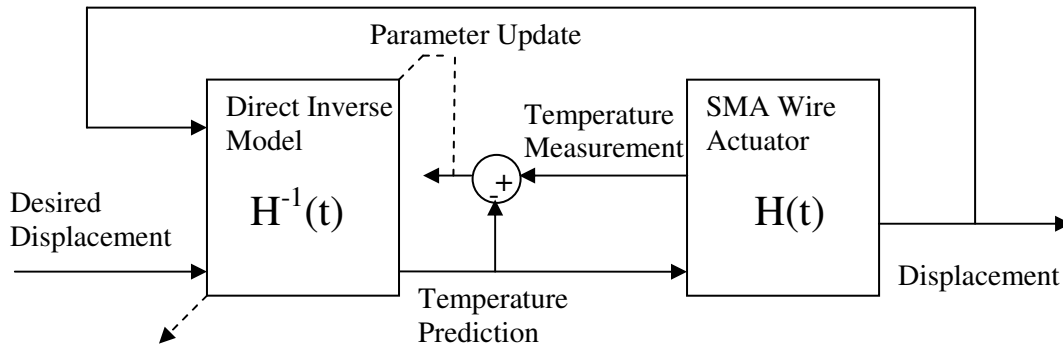Fig. 20. Schematic diagram of adaptive control methodology

Generally, many researches find the hysteresis model $H(t)$ adaptively and obtain the inverse model $H^{-1}(t)$ of it for tracking control[15],[25],[26]. They used output-based adaptive control. This means that the output error is used for the adaptation. However, in our case, the hysteresis model $H(t)$ is not required, and the inverse model $H^{-1}(t)$ is

directly obtained by using an adaptive identification technique. Now, the input for the model is displacement of SMA and the output is temperature. Fig. 20 illustrates the concept of this adaptive controller. The adaptive inverse model is described as two ways. One is the adaptive KP model and the other is the inverse model with an orthogonal polynomial network. Each adaptive inverse model is continuously updated online to minimize the error between the temperature measurement and temperature continuously updated reference. Temperature prediction with respect to the input of a desired displacement is obtained from the direct inverse model. As a result, these adaptive inverse models can predict the hysteresis of SMA wire actuator and compensate for the hysteretic behavior.

The difference between the adaptive direct model with KP model and the inverse model with an orthogonal polynomial network is only the model representation. As a method to update the model, the gradient algorithm is applied to both models.

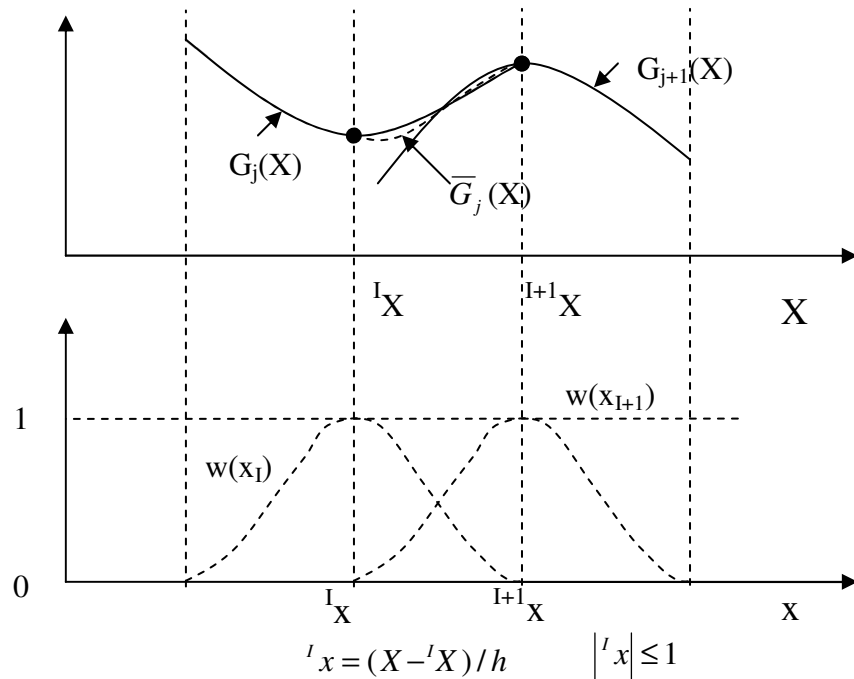*E. Adaptive Inverse Model by using Orthogonal Polynomial Network*

Fig. 21. Weighting function approximation of a one-dimensional function

A Global-Local Orthogonal Polynomial Mapping(GLO-MAP) network has the good applications to input-output function approximation[27]. Basically, a GLO-MAP network consists of weighting functions and local approximations. The local approximations are selected as the linear combinations of a set of basis functions which are orthogonal with respect to the weighting functions. For one dimensional case, weighted average approximation is written as

$$\overline{G}_I(X) = w(^Ix)G_I(X) + w(^{I+1}x)G_{I+1}(X), \text{ for } 0 \leq ^Ix < 1 \tag{35}$$

where the weighting functions $w(x)$ used to average the two adjacent preliminary local approximations, $G_I(X)$ and $G_{I+1}(X)$. Also, X represents the global coordinate and x is the local coordinate. Fig. 21 shows this approximation graphically for a one-dimensional function. After choosing the weight functions and basis functions shown in table 2[27], each coefficient of the basis functions can be updated by learning law through the input-output data. For our inverse problem, gradient learning algorithm is used for obtaining the coefficients of the basis functions.

Table 2

One Dimensional Basis Functions Orthogonal with Respect to the Weight Function

$$w(x) = 1 - x^2(3 - 2|x|)$$

degree	Basis Functions, $\phi_j(x)$
0	1
1	x
2	$(-2 + 15x^2)/13$
3	$(-9x + 28x^3)/19$
⋮	⋮
n	$\phi_n(x) = \dfrac{1}{c_n}\left[x^n - \displaystyle\sum_{j=0}^{n-1} \dfrac{<x^n, \phi_j(x)>}{<\phi_j(x), \phi_j(x)>}\phi_j(x)\right]$

The inverse function can be approximated as

$$\overline{g}_I(X) = w({}^I x)g_I(X) + w({}^{I+1}x)g_{I+1}(X), \text{ for } 0 \leq {}^I x < 1 \tag{36}$$

$$\overline{g}_I = C^T W \tag{37}$$

where

$$C = [c1 \quad c2 \quad c3 \quad c4 \quad c5 \quad c6 \quad c7 \quad c8]^T$$

$$W = \begin{bmatrix} w({}^I x)\phi(1) \\ w({}^I x)\phi(2) \\ w({}^I x)\phi(3) \\ w({}^I x)\phi(4) \\ w({}^{I+1}x)\phi(1) \\ w({}^{I+1}x)\phi(2) \\ w({}^{I+1}x)\phi(3) \\ w({}^{I+!}x)\phi(4) \end{bmatrix} = \begin{bmatrix} (1 - x^2(3 - 2|x|)) \times 1 \\ (1 - x^2(3 - 2|x|)) \times x \\ (1 - x^2(3 - 2|x|)) \times (-2 + 15x^2)/13 \\ (1 - x^2(3 - 2|x|)) \times (-9x + 28x^3)/19 \\ (1 - (x-1)^2(3 - 2|x-1|)) \times 1 \\ (1 - (x-1)^2(3 - 2|x-1|)) \times x \\ (1 - (x-1)^2(3 - 2|x-1|)) \times (-2 + 15x^2)/13 \\ (1 - (x-1)^2(3 - 2|x-1|)) \times (-9x + 28x^3)/19 \end{bmatrix}$$

$$w({}^I x) = (1 - x^2(3 - 2|x|)), \quad w({}^{I+1}x) = (1 - (x-1)^2(3 - 2|x-1|))$$

$$\phi(1) = 1, \quad \phi(2) = x, \quad \phi(3) = (-2 + 15x^2)/13, \quad \phi(4) = (-9x + 28x^3)/19$$

For the estimation of coefficient C, the estimator is generated as

$$\hat{\overline{g}}_I = \hat{C}^T W \tag{38}$$

where $\hat{C}$ is the estimate of C at each time t. The normalized estimation error ε is created as

$$\varepsilon = \frac{\overline{g}_I - \hat{\overline{g}}_I}{m^2} \tag{39}$$

where $m^2 = 1 + n_s$ and $n_s = W^T W$. By applying the gradient algorithm, the adaptive law is following as

$$\dot{\hat{C}} = \Gamma \varepsilon W \tag{40}$$

The input is the displacement of the SMA actuator, and the temperature is the output of the inverse model. So, the displacement of the SMA actuator is X variable, and the temperature is $\overline{g}_I(X)$ in Eq. (36).

At each running time, we can approximate the adaptive inverse model of the SMA output and the temperature. From this inverse model, corresponding temperature with respect to the desired displacement of SMA actuator can be obtained.
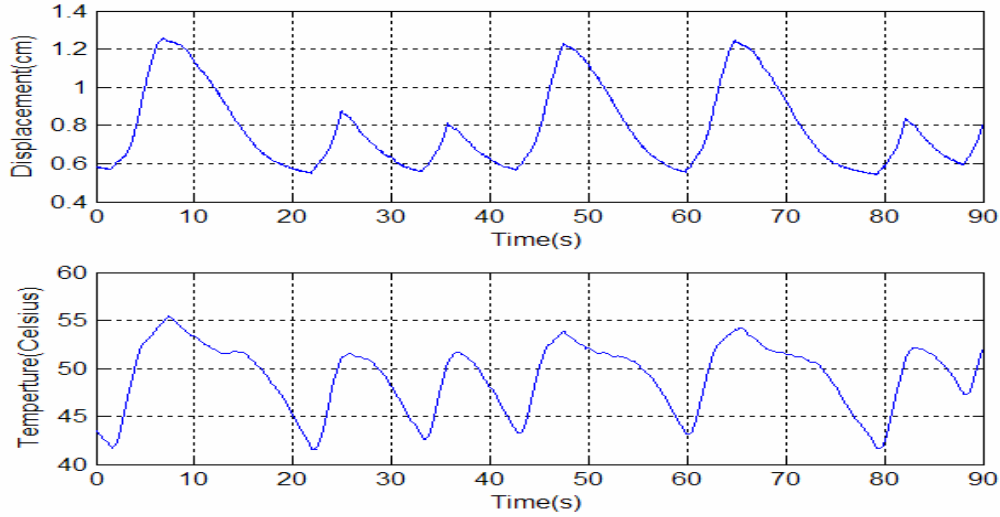
F. Simulation Study

Fig. 22. One input-output data set from SMA experiment

One input-output data set obtained from the experiment in Fig. 22 is used to get the inverse model. This describes the relationship between temperature and displacement of the SMA wire actuator. Two inputs and two outputs are used: {Displacement of the SMA actuator, Variation of displacement} and {Temperature, Variation of temperature}. The range of the input is in $0 \leq^I x < 1$. So, modified input set is used by scaling such as {Displacement of SMA actuator/1.5, Variation of displacement/10}. $10I_{8X8}$ and $0.15I_{8X8}$ are used for the adaptation gain.

Two inverse models are represented with displacement and temperature, and with the variation of displacement and the variation of temperature, respectively, as

$$\overline{g}_{I1}(X_1) = C_1^T W_1 \tag{41}$$

$$\overline{g}_{I2}(X_2) = C_2^T W_2 \tag{42}$$

These models can update by the adaptive law described in Eq. (40).

G. Simulation Results

Fig. 23 shows that the inverse model control with an orthogonal polynomial network has a good tracking for the reference. This inspiring result gives a possibility for real-time control. The results of on-line inverse model control will be shown in the next section. Fig. 24 shows that it is hard for the second inverse model to follow the variation of the displacement. Because the error between experimental data and the inverse data in second inverse model is bounded and the main interest is the displacement, this result is reasonable for our control problem.
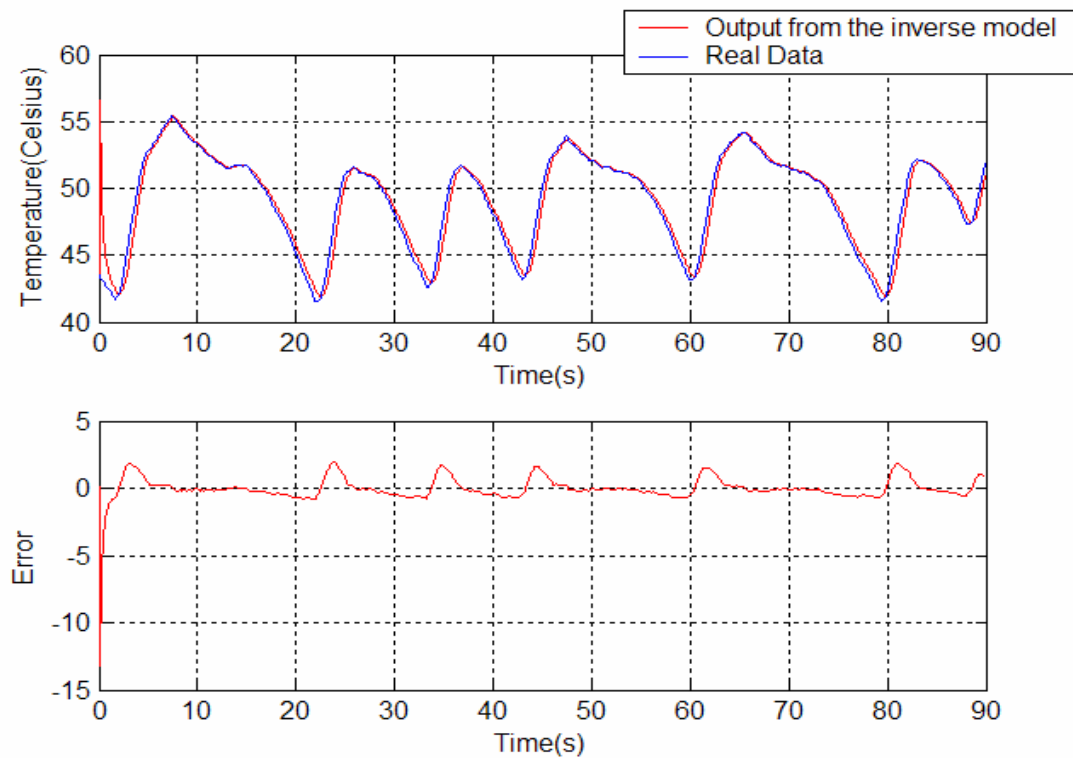

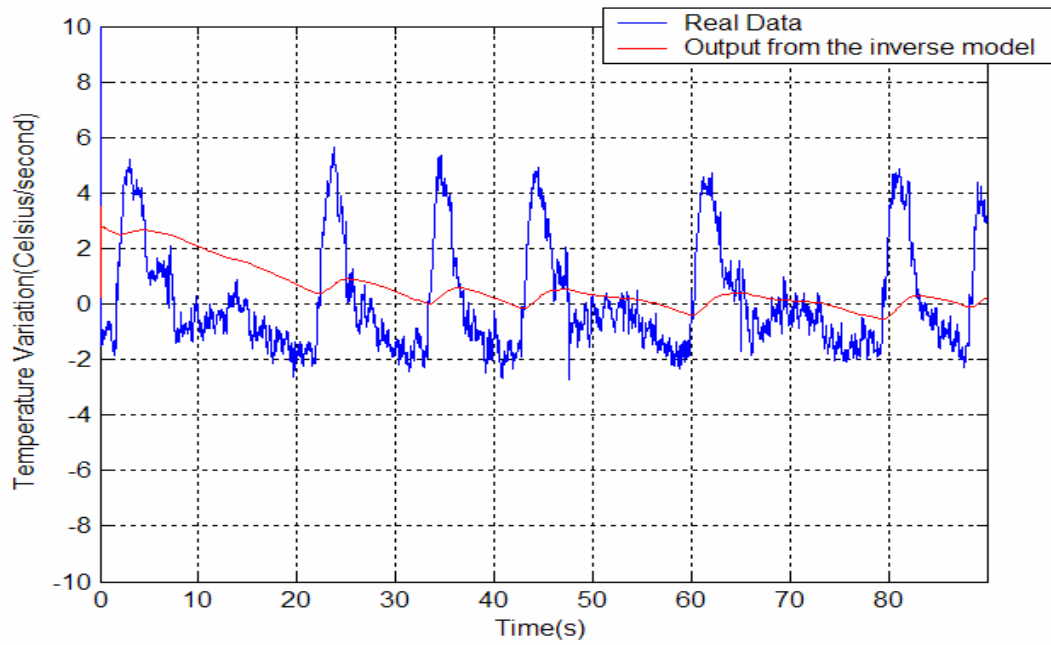Fig. 23. Temperature and output from adaptive inverse model

Fig. 24. Displacement variation and output from adaptive inverse model
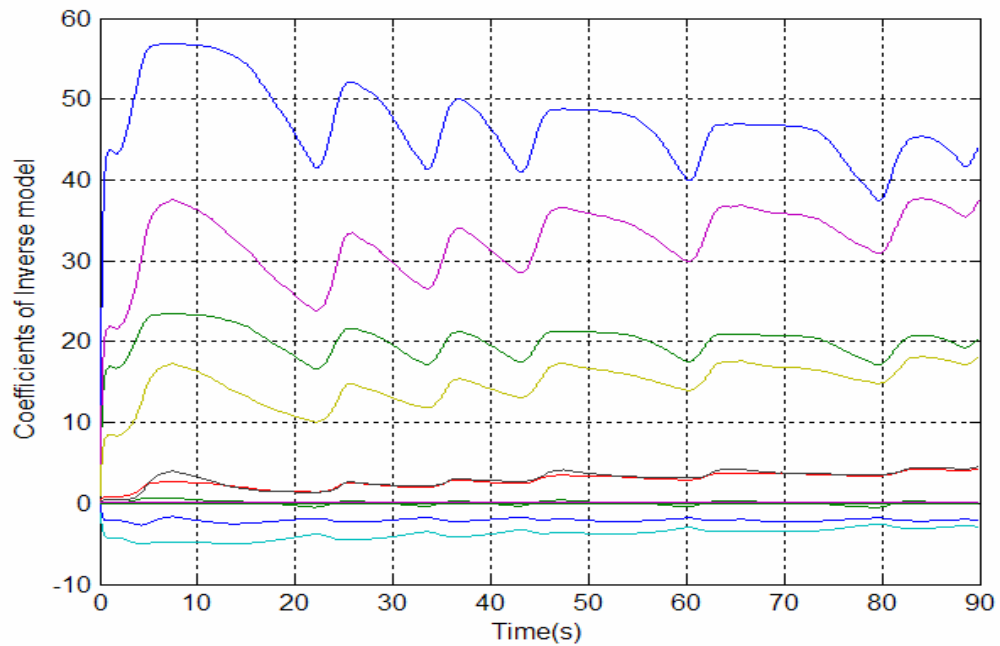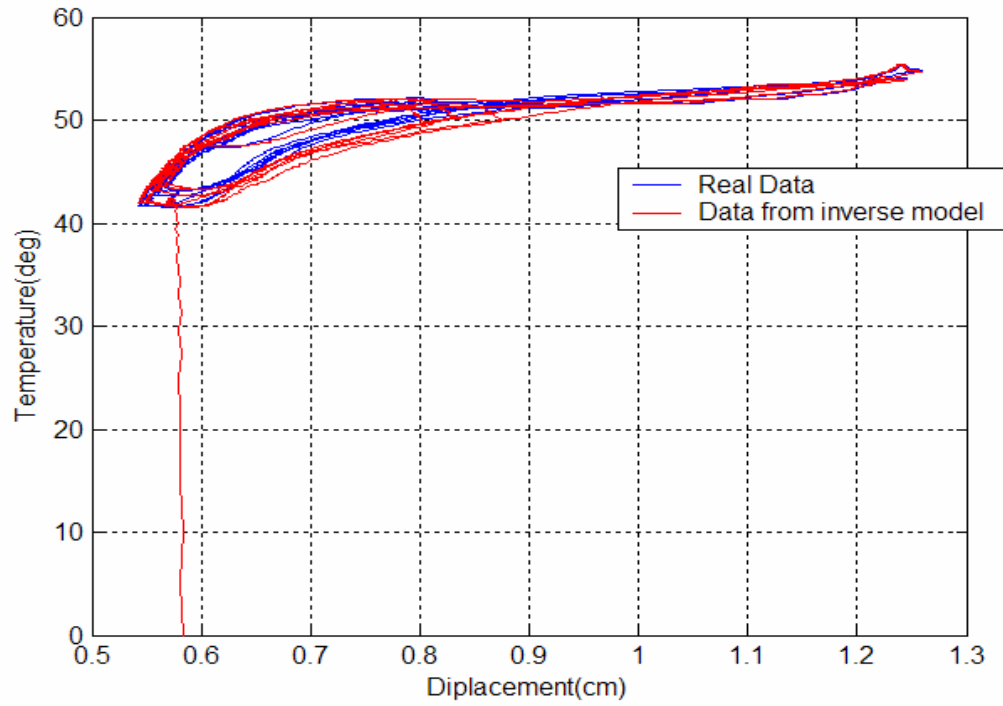

Fig. 25. Coefficients of inverse model

Fig. 26. Input-output relationship in the inverse model

Fig. 25 shows the coefficients of the inverse model. Each coefficient is bounded in the some range. Fig. 26 shows that the relationship between the input and output of the inverse model is almost same as the experimental data.

CHAPTER VI

EXPERIMENTAL RESULTS

A. Adaptive Identification of the Direct Inverse KP Model

To get the direct inverse model with the KP hysteresis model, first, the shape and the movement direction of hysteresis should be validated experimentally. As mentioned before, this gives us an insight into the range of reasonable values for the weight function. If the hysteresis behavior obtained from the experiment is like Fig. 2(a), each discretized point in the KP plane may have the positive values in weight function. Whereas, if the hysteresis is like Fig. 2(b), each discretized point follows the properties mentioned in chapter III. When we use the displacement as the input and the temperature as the output for the direct inverse model, Fig. 27 shows that the hysteresis is like Fig. 2(a). Point ⓐ and ⓑ represent the position at t=50secs and t=65secs, respectively. Therefore, each value of the weight function has mostly the positive value in our case. This information will be used for the gradient method with projection.
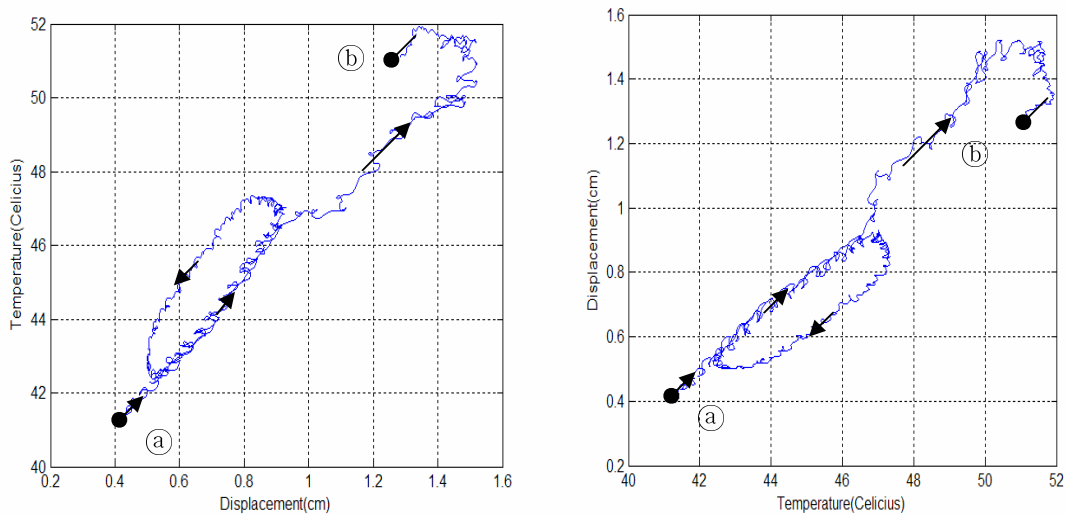
Fig. 27. Relationship between temperature and displacement

Moreover, there are several design parameters for KP model to be chosen carefully. With these parameters, the adaptive KP model will be obtained.

a) Parameterization number K

This number decides the number of grids in the vertical or horizontal line over the Preisach plane. If K is large, the parameterized KP model acts like the integral KP model. However, there is computational cost for large K so that a proper K should be considered. For our experiment, 10 is selected for K.

b) Parameter a of ridge function in KP kernel

This decides the curve shape of the ridge function. The optimal rise constant is determined as

$$a_{opt} = \frac{u_{max} - u_{min}}{K - 1} \tag{43}$$

where u_{max} and u_{min} represent the maximum and minimum input values[15].

c) Input Range

This is the range of the SMA displacement. The range should cover the entire SMA displacement. So, it is from 0 to 1.8 in case of this experiment.

d) The adaptive law

Each θ_{ij} of weight function has a priori: θ_{ij} is greater than 0. This information is used for gradient algorithm with the projection. The adaptive gain is chosen by 10.

Fig. 28 represents the comparison between the SMA output and the output of the adaptive KP model. The adaptive KP model can follow the SMA output perfectly. Fig. 29 shows that the fixed KP model with parameters obtained from the adaptive KP model after 123 seconds can also predict the hysteresis behavior with reasonably small error. Hysteresis responses of the adaptive KP model and the fixed KP model are described in Fig. 30. The weight function of the fixed KP model is described in Fig. 31 and Table 3.

This fixed KP model also can be used as the feed-forward model for the SMA position control.
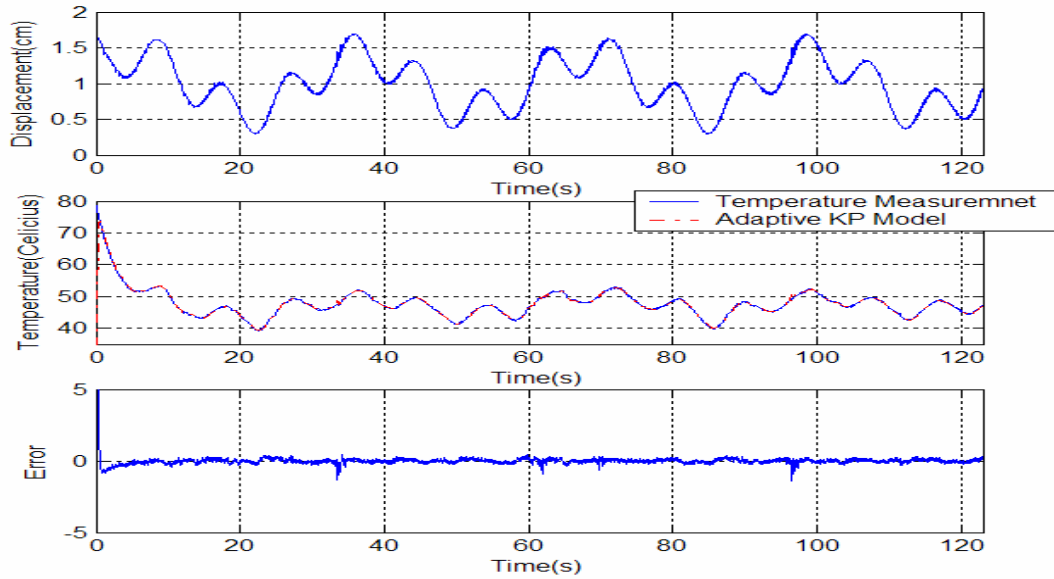

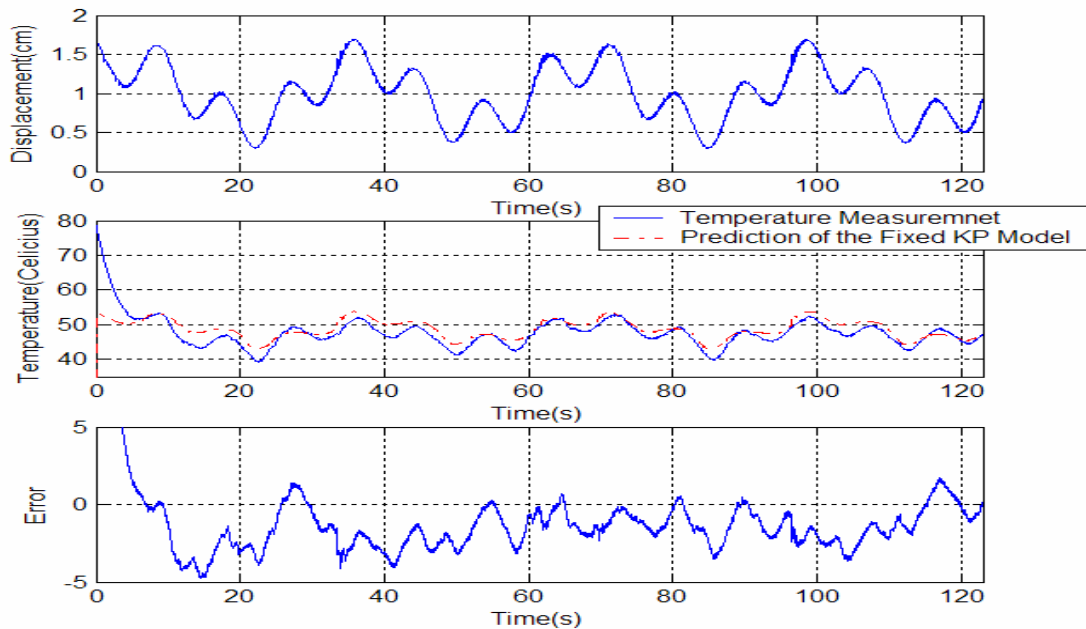Fig. 28. Comparison between SMA output and the adaptive KP model

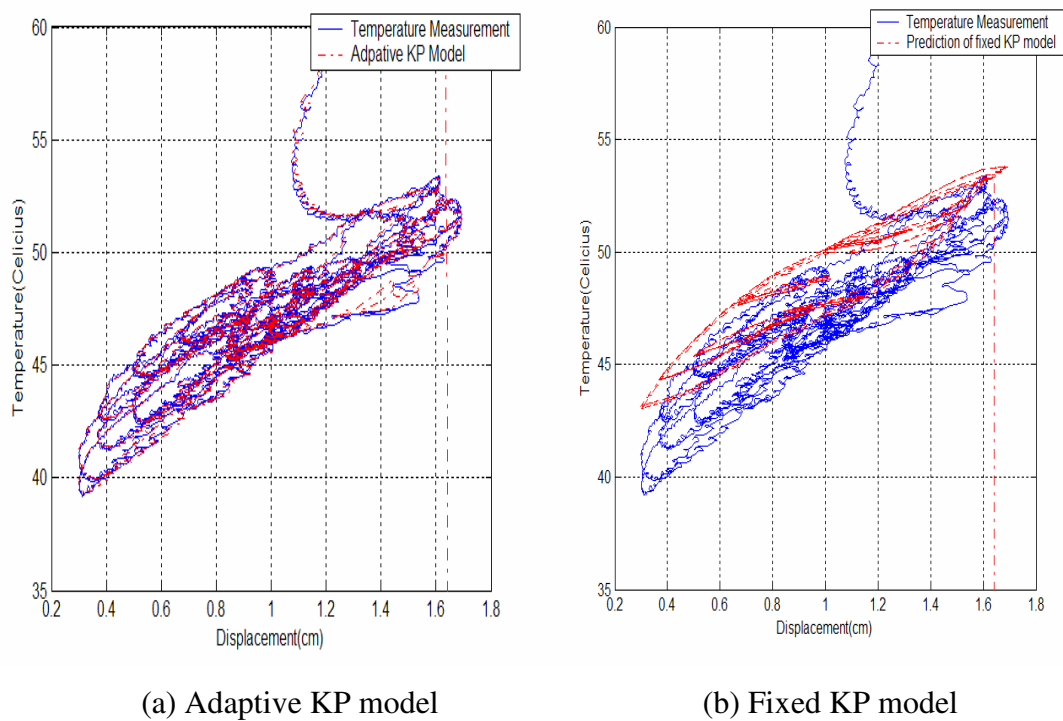Fig. 29. Comparison between SMA output and fixed KP model after 123 seconds

(a) Adaptive KP model   (b) Fixed KP model
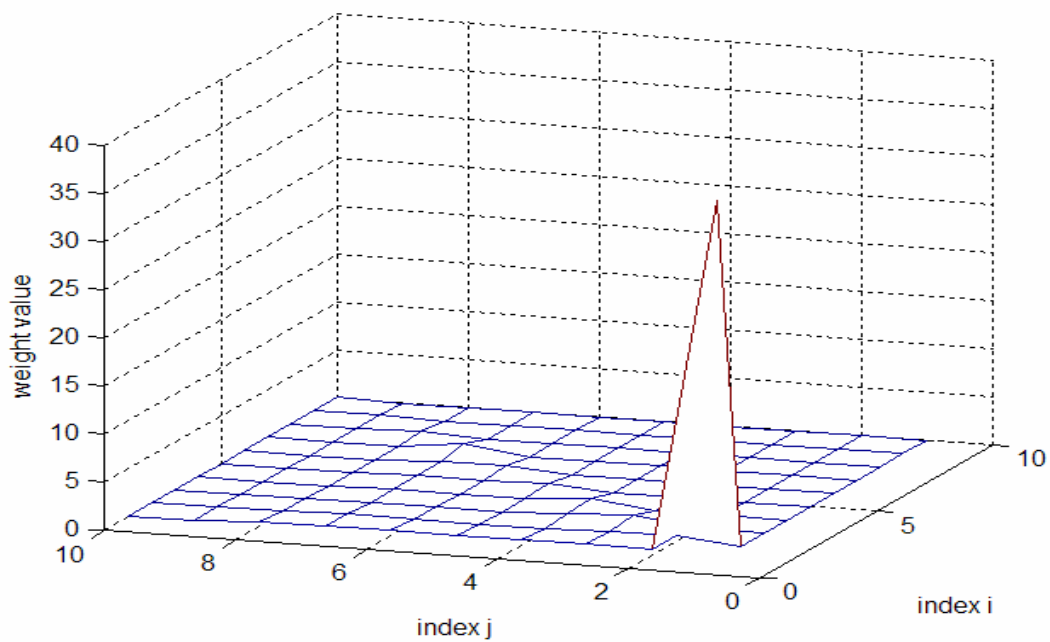
Fig. 30. Hysteresis response

Fig. 31. Weight values after adaptation of 123 seconds

Table 3

Estimated Weight Values after Adaptation of 123 Seconds

| Index j Index i	1	2	3	4	5	6	7	8	9	10
1	37.4057	0.5529	0.5529	0.5529	0.5529	0.5529	0.5529	0.5529	0.2292	0.100
2	0	0.6715	0.5637	0.4588	0.4006	0.3857	0.4155	0.4494	0.2292	0.100
3	0	0	0.8661	0.5023	0.2305	0.1909	0.2372	0.2943	0.1756	0.100
4	0	0	0	0.7132	0.2988	0.1681	0.2195	0.2646	0.1613	0.100
5	0	0	0	0	0.4433	0.1742	0.2074	0.2497	0.1468	0.100
6	0	0	0	0	0	0.3722	0.3078	0.4049	0.1488	0.100
7	0	0	0	0	0	0	0.5642	0.6702	0.2207	0.100
8	0	0	0	0	0	0	0	0.9260	0.2843	0.100
9	0	0	0	0	0	0	0	0	0.2806	0.100
10	0	0	0	0	0	0	0	0	0	0.100

B. Comparison among Controllers

In order to test three controllers for real-time tracking control, step and sinusoidal response are applying to the SMA wire actuator: regular PI controller, adaptive controller with KP model and adaptive controller with an orthogonal polynomial network. However, regular PI controller give both adaptive controllers have the PID controller for the temperature control. Both adaptive controllers are implemented by using S-function in Matlab/simulink.

1) Step Response

Fig. 32 shows the step response of SMA wire actuators and the performance of SMA wire actuator. The rise time is within 1 second and the cooling time is around over 4 seconds. If one of the cooling methods mentioned in chapter II is used, this cooling time reduces. All controllers have a reasonable good tracking result. The adaptive controller with the KP model exhibits the shortest overshoot. The adaptive controller with an orthogonal polynomial network has slightly worse tracking result than others.
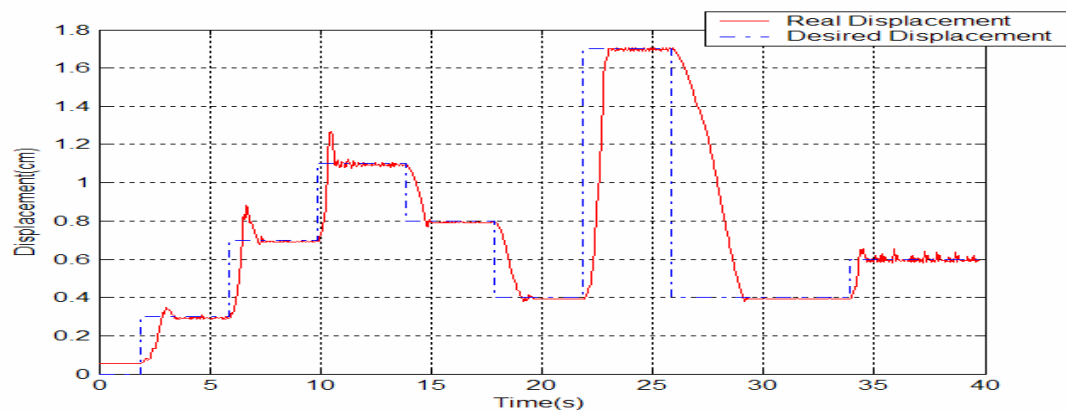
(a) PI controller
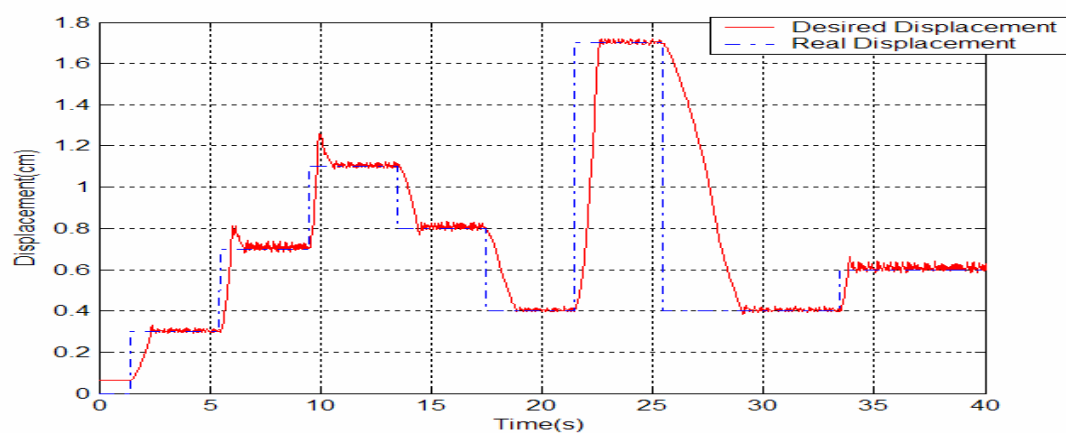
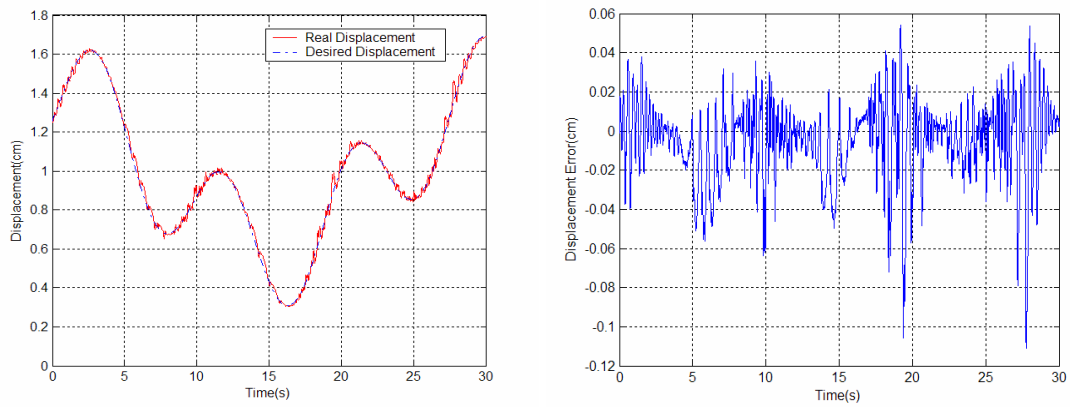(b) Adaptive controller with KP model
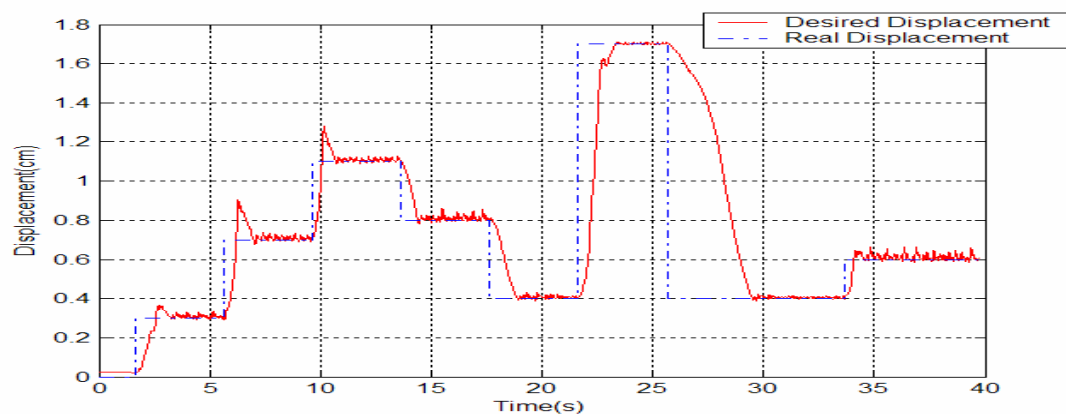
(c) Adaptive controller with an orthogonal polynomial network

Fig. 32. Step response

2) Sinusoidal Response

Fig. 33 represents the sinusoidal response of SMA wire actuators. To compare the performance of controllers, the RMS error and maximum error are given in Table 4. According to Table 4, the adaptive controller with the KP model has the smallest value in RMS and maximum error, whereas the adaptive controller with an orthogonal polynomial network has the largest error. This means that the adaptive inverse model with the KP model predicts the temperature well with respect to the desired displacement. However, all controllers have good performance in the sinusoidal response.

(a) PI controller
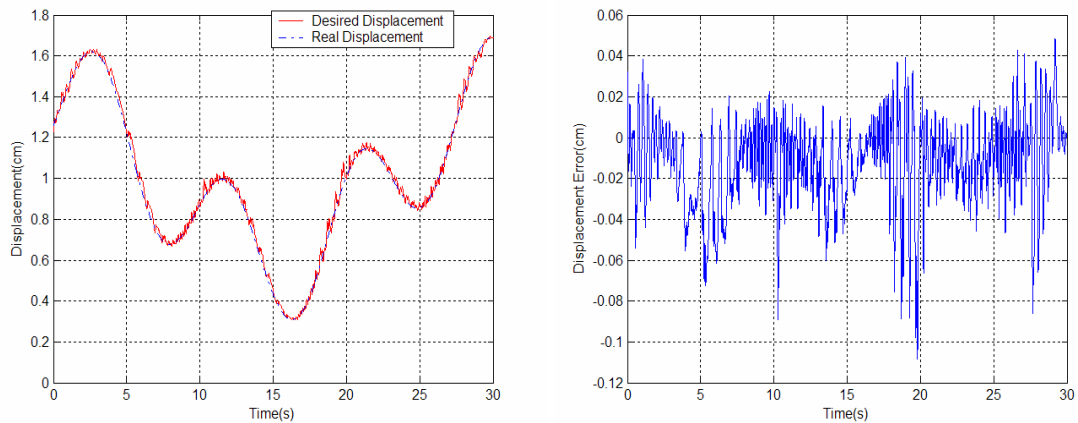
(b) Adaptive controller with KP model

Fig. 33. Sinusoidal response
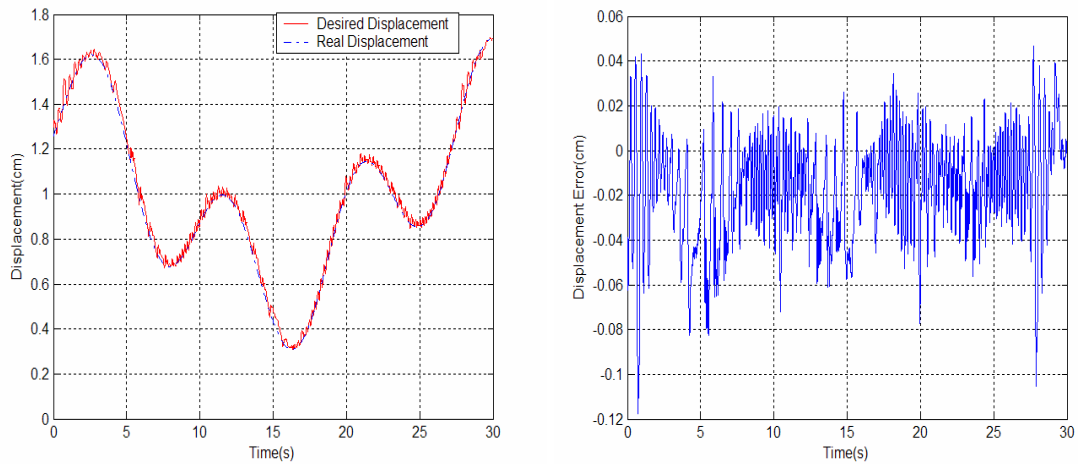
(c) Adaptive controller with an orthogonal polynomial network

Fig. 33. Continued.

Table 4

Comparison of Tracking Error

	PI	KP model	O.P.Network
RMS tracking error(cm)	0.027	0.0248	0.0287
Maximum tracking error(cm)	0.1111	0.1083	0.1176

As mentioned before, both adaptive inverse controllers have the PI controller for the temperature control. If the temperature control is improving, more good tracking results are expected.

CHAPTER VII

CONCLUSIONS

The characteristics of an SMA wire actuator are studied in order to obtain the guidance for selection of the SMA wire actuators for appropriate applications. To compensate for the effect of the hysteresis behavior of an SMA wire actuator in tracking control, we use the adaptive inverse model of an SMA wire actuator based upon the KP hysteresis model. This is done in order to avoid the inverse operation because the inverse of hysteresis behavior also has qualitatively the same characteristics of hysteresis.

These Preisach types of models require many computations and a lot of memory because of their complex model structures. So, we propose the nonlinear adaptive inverse model control by using an orthogonal function approximation to control the SMA displacement. This proves to be a more compact and computational attractive approach.

Finally, a PI controller, an adaptive controller with the KP model and an adaptive nonlinear inverse model controller with an orthogonal polynomial network are compared experimentally. The adaptive controller with the KP model has the shortest overshoot in the step response and the smallest RMS error in the sinusoidal response. The adaptive controller with an orthogonal polynomial network has slightly worse tracking results than other controllers, but the results are acceptable.

REFERENCES

[1] M. Hashimoto, M. Takeda, H. Sagawa, I. Chiba, and K. Sat, "Shape memory alloy and robotic actuators," *J. Robot. Syst.,* vol. 2, no. 1, pp. 3-25, January 1985.

[2] K. Ikuta, "Micro/miniature shape memory alloy actuator," in *Proc. 1990 Int. Conf. Robot. Automat.*, Cincinnati, May 13-18, pp. 2156-2161.

[3] J. N. Kudva., "Overview of the DARPA Smart Wing Project," *J. Intell. Material Syst. Struct.*, vol. 15, pp. 261-267, April 2004.

[4] Friedrich K. Straub, Dennis K. Kennedy, David B. Domzalski, Ahmed A. Hassan, Hieu Ngo, V. Anand And Terry Birchette, "Smart Material-actuated Rotor Technology – SMART," *J. Intell. Material Syst. Struct.*, vol. 15, pp. 249-260, April 2004.

[5] K. Ikuta, M. Tsukamoto, and S. Hirose, "Mathematical model and experimental verification of shape memory alloy for designing microactuator," in *Proc. 1991 Micro Electro Mechanical Syst. (MEMS '91),* January 30-February 2, pp. 103-108.

[6] Daniel R. Madill and David Wang, "Modeling and L2-Stability of a Shape Memory Alloy Position Control System," *IEEE Trans. Control Syst. Technol.*, vol. 6, no. 4, pp. 473-481, July 1998.

[7] L. C. Brinson, A. Bekker, and S. Hwang, "Deformation of shape memory alloys due to thermo-induced transformation," *J. Intell. Material Syst. Struct.*, vol. 7, pp. 97-107, January 1996.

[8] Sumiko Majima, Kazuyuki Kodama, and Tadahiro Hasegawa, "Modeling of shape memory alloy actuator and tracking control system with the model," *IEEE Trans. Control Syst. Technol.*, vol. 9, no. 1, pp. 54-59, January 2001.

[9] Glenn V. Webb and Dimitris C. Lagoudas, Andrew J. Kurdila, "Hysteresis modeling of SMA actuators for control applications," *J. Intell. Material Syst. Struct.*, vol. 9, pp. 432-448, June 1998.

[10] G. Webb and D. Lagoudas, A. Kurdila, "Adaptive hysteresis compensation for SMA actuators with stress-induced variations in hysteresis," *J. Intell. Material Syst. Struct.*, vol. 10, pp. 845-854, November 1999.

[11] C. M. Wayman and T. W. Duerig, "An introduction to Martensite and Shape Memory," *Engineering Aspects of Shape Memory Alloys*, T. W. Duerig, et al., Eds., Boston : Butterworth-Heinemann, p10, 1990.

[12]   DYNALLOY, Inc., Flexinol® Technical Data,

http://www.dynalloy.com/TechnicalData.html, Accessed : May 2006.

[13] M. Hashimoto, M. Takeda, H. Sagawa, I. Chiba and K. Sato, "Application of shape memory alloy to robotic actuators," *J. Robotic Syst.*, vol. 2, no. 1, pp. 3-25, January 1985.

[14] I. Mayergoyz, *Mathematical Models of Hysteresis*. Berlin: Springer-Verlag, 1991.

[15] G. Webb, "Adaptive Identification and Compensation For a Class of Hysteresis Operators," PhD Dissertation, Texas A&M University, College Station, May 1998.

[16] M. M. Khan, D. C. Lagoudas, J. J. Mayes and B. K. Henderson, "Pseudoelastic SMA spring elements for passive vibration isolation: Part I - modeling," *J. Intell. Material Syst. Struct.*, vol. 15, pp. 415-441, June 2004.

[17] D. Hughes and J. Wen, "Preisach modeling and compensation for smart material hysteresis," *SPIE Active Materials and Smart Structures,* vol. 2427, pp. 50-64, January 1994.

[18]. M. Krasnoselskii and A. Pokrovskii, *Systems with Hysteresis*, Mocow : Nauka, 1983.

[19] H.T. Banks, A.J. Kurdila and G. Webb, "*Identification of Hysteretic Control Influence Operators Representing Smart Actuators Part I: Formulation*," Tech. Rep. CRSC-TR96-14, Center for Research in Scientific Computation, North Carolina State University, Raleigh, N.C., 1996.

[20] H.T. Banks, A.J. Kurdila and G. Webb, "*Identification of Hysteretic Control Influence Operators Representing Smart Actuators Part II: Convergent Approximations*," Tech. Rep. CRSC-TR97-7, Center for Research in Scientific Computation, North Carolina State University, Raleigh, N.C., 1997.

[21] S. Sastry and M. Bodson, *Adaptive Control: Stability, Convergence, and Robustness*, Englewood Cliffs, NJ : Prentice-Hall, 1989.

[22] P. Ioannou and J. Sun, *Robust Adaptive Control*, Englewood Cliffs, NJ : Prentice-Hall, 1996.

[23] J. McNichols and J. Cory, "Thermodynamics of nitinol," *J. Appl. Phys.,* vol. 61, no. 3, pp. 972-984, February 1987.

[24] Sushant M. Dutta and Fathi H. Ghorbel, "Differential hysteresis modeling of a shape memory alloy wire actuator," *IEEE/ASME Trans. Mechatronics*, vol. 10, no. 2, pp. 189-197, April 2005.

[25]   Xiaobo Tan, John S. Baras, "Adaptive identification and control of hysteresis in smart materials," *IEEE Trans. Automatic Control*, vol. 50, no.6, pp. 827-839, June 2005.

[26] G. Song, J. Zhao, X. Zhou, and J. Abreu-Garcia, *"*Tracking control of a Piezoceramic actuator with hysteresis compensation using inverse Preisach model*," IEEE/ASME Trans. Mechatronics*, vol. 10, no. 2, pp. 198-209, April 2005.

[27]   J. L. Junkins, P. Singla, D. T. Griffith and T. Henderson, "Orthogonal Global/Local Approximation in N-dimensions: Applications to Input-Output Approximation," *6th International conference on Dynamics and Control of Systems and Structures in Space*, Cinque-Terre, Italy, 2004.

APPENDIX A

CURRENT AMPLIFIER AND TEMPERATURE MEASUREMENT CIRCUIT
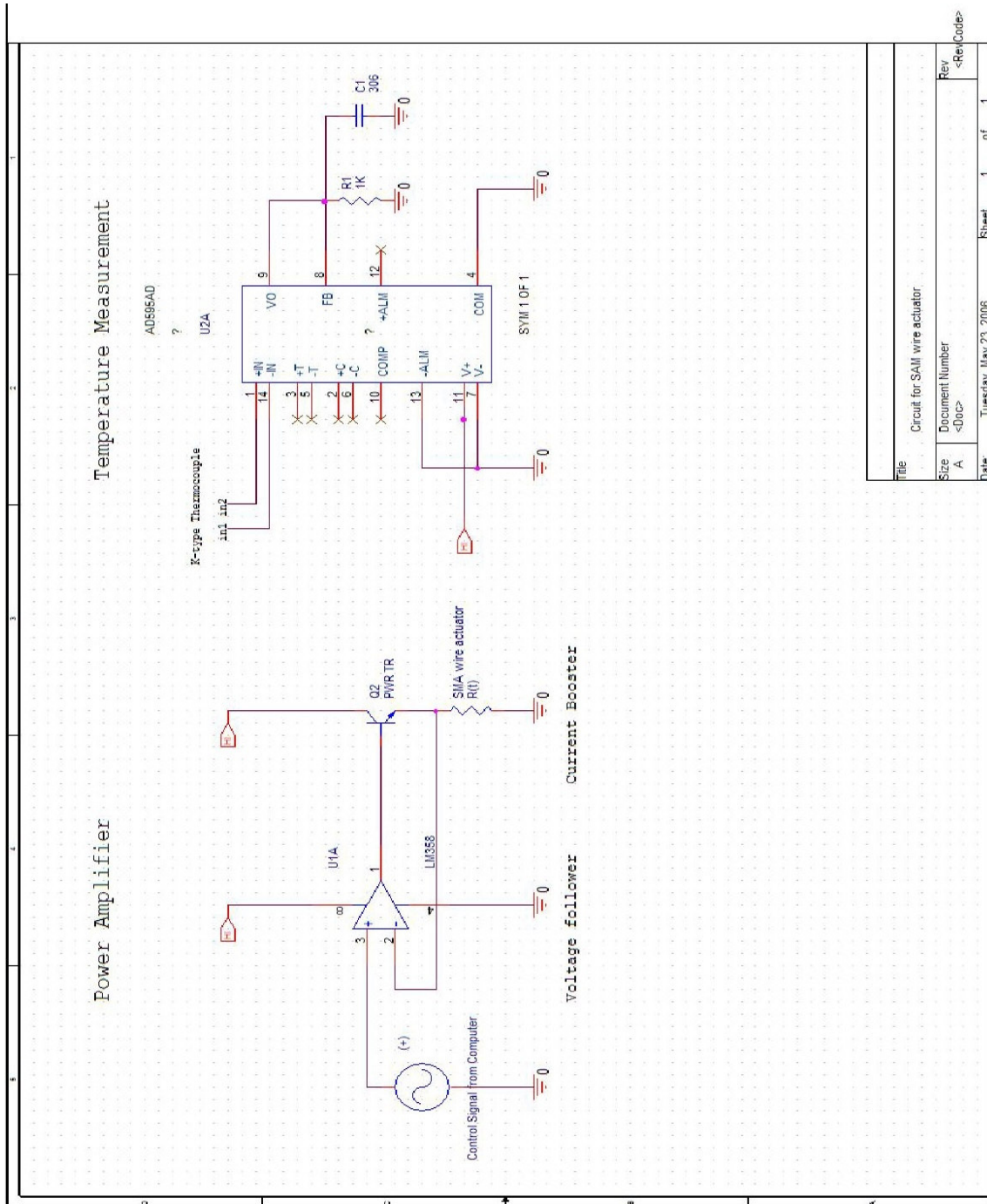
VITA

Bong Su Koh was born in Jeju, the Republic of Korea, on May 1, 1977. He received his Bachelor of Science degree in aerospace engineering and electrical engineering at the Korea Advanced Institute of Science and Technology in Daejeon, Republic of Korea, in February, 2003. He studied for his Master's degree in aerospace engineering at Texas A&M University under Dr. John L. Junkins. He received his M.S. degree in August 2006. His major specialization is dynamics and controls in the field of aerospace engineering. His permanent address is 314-47 Yeon-Dong Jeju, Korea.